END
DATE
FILMED
8-83
DTIC

MICROCOPY RESOLUTION TEST CHART
NATIONAL BUREAU OF STANDARDS-1963-A

1 June 1982

THEORETICAL AND SEMI-EMPIRICAL METHODS

OF DESIGNING RIBBON UNWINDERS

FINAL REPORT: Contract DAAK10-80-C-0297

For: DEPARTMENT OF THE ARMY

          U.S. ARMY ARMAMENT R&D COMMAND

          SMALL CALIBER WEAPON SYSTEMS LABORATORY

          DOVER, NEW JERSEY 07801

By: 3C Systems, Inc.

          620 Argylé Road

          Wynnewood, Pa. 19096

          Hamilton Technology, Inc.

          Lancaster, Pa.

          Adaptronics, Inc.

          McLean, Va.

83 06 30 046

TABLE OF CONTENTS

1.   INTRODUCTION & SUMMARY

The objective of this program has been to develop
theoretical and semi-empirical methods to enable engineers
to design ribbon unwinders with reasonable accuracy and a
minimum of development effort.   This basic objective has
been fulfilled, despite the fact that the degree of pre-
dictive accuracy depends to some extent on the design
details of the fuze containing the ribbon unwinder. → *coverleaf 1*
Fig. 1 illustrates this point in relation to application
of the unwinder principle to the XM579 Fuze.

Fig. 1 contains a cross-section (Section B-B) of
the XM579 unwinder prior to spin-up.   The ribbon is shown
unrestrained, with a short length of its end free.   There
are surface adhesion forces developed during the ribbon
winding process that are high enough to permit the coils
to be handled in this manner, depending on ribbon material
and surface finish and on winding tightness.   When the
projectile is fired, setback accelerations and friction
provide the means whereby the ribbon coil is spun up·to
the projectile's rotation rate, and the tightness of a
coil wound in the proper direction (opposite to the
direction of spin) will increase during the spin-up
period.   After the spin-up period, centrifugal forces
serve to unwind the coil and transfer it from the hub
radially outward to the housing.   When the detent pin
is released by the innermost coil of the ribbon, it
tumbles outward thereby releasing the rotor, which is
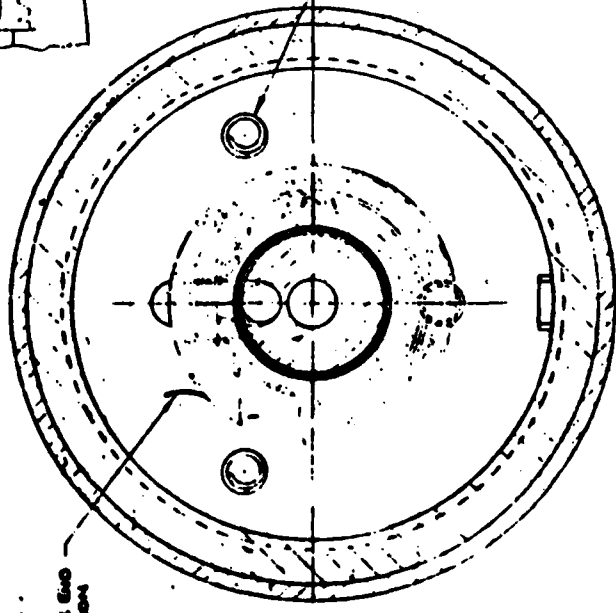turned to the armed position by centrifugal force.

Although winding tightness has been found not to
be a significant parameter affecting arming time, and

- 1 -

FIG. 1 XM579 FUZE

SECTION A-A

SECTION B-B

- 2 -

therefore the added tightening due to spin-up is expected
not to be significant, the XM579 design feature of using
a detent pin is expected to influence unwinding time.
In the course of experimentation on this program, analysis
of high speed films showed clearly that the radial pressure
of the split-ring-hub used in the tests was the cause of
some additional time delay, of the order of 10 milliseconds,
after all but the innermost ribbon coil had been transferred
out to the housing. It is therefore expected that the XM579
detent pin will provide a different time delay at the end
of ribbon unwinding. For practical reasons like this, then,
one cannot expect to develop completely general predictive
equations for ribbon unwinding time, applicable to all fuze
designs. Furthermore, if the ribbon is used to generate
energy or to actuate other arming mechanisms, the external
forces can be expected to result in additional time delays.
Fortunately, however, practical delay systems can be designed
without introducing excessive time delays above those provided
by the pure unwinding process.

In order to fulfill the program objectives, a three-
pronged investigation was undertaken, as follows:

(1) An experimental program employing wide variations
in the parameters that affect ribbon unwinder performance.
.These parameters involved the ribbon geometric factors of
thickness, width, length, hub radius and cavity radius;
ribbon material parameters of density, modulus of elasticity,
heat treatment, friction coefficient; loading factors of
centrifugal loading and axial forces. It was originally
planned to modify XM579 fuzes and fire them in 30mm rounds,
in order to include any effects of axial loads during
setback.* However, the modifications required to provide

---

* It was anticipated that very thin, very soft ribbons like
  lead might have their edges distorted during setback.

in-flight indications of the completion of arming were
found to be far more expensive than this program could
afford. Accordingly, the program objectives were accom-
plished in the laboratory using a high-speed air spinner.
This change in experimental approach had its compensating
virtue of permitting photographic observation of the
ribbon dynamics as they unwound.

(2) A multivariate regression computer analysis of
the experimental results in order to identify(on the basis
of data alone, not theoretical nor intuitive expectations)
critical parameters and combinations of parameters that
could not be studied by analytical methods. Besides
identification, this computational approach can quantify
the dependency of ribbon unwinding time on these parameters
for use in design.

(3) A theoretical analysis to obtain predictive
equations involving the key parameters that affect unwinder
performance. In a sense, this approach of analyzing the
physics of unwinding and the above approach of computer
analysis of experimental data alone could be considered
competitive, perhaps yielding identical results. In practice,
however, the approaches complement one another. The physical
analysis can develop the general form of the unwinding time
equation, including parameters that are not varied during
the test series (in this instance, for example, hub radius
and cavity radius were held constant), while the data-alone
analysis cannot indicate the effects of parameters that are
not varied. Multivariate regression analysis of the data
does, on the other hand, include the effects of parameters
that exist during testing but are not included in the
physical analysis. Variations in test procedures and
parameters that the physical analyst either could not

include in the analysis or did not expect to be important, may be uncovered by the multivariate regression analysis of the test data.

Selection of parameters for testing and analysis was made after study of the literature available on previous ribbon unwinder programs. Ref. 3 provided background on coiled steel ribbons that were attached to a high inertia pointer to indicate unwinding time. Because these ribbons functioned as springs and because of the high external inertia loading, these data could not be applied to the current unwinder program which uses unloaded, dead-soft ribbons.

Ref. 2 contains some useful data on brass ribbons fired at about 75,000 rpm in 20mm projectiles at heavy aluminum targets designed to stop the round's rotation on impact and to permit recovery of the unwinder ribbons. Fig. 2 contains these data. The approximately linear shapes of the curves in Fig. 2 are in agreement with those observed in this current program using high speed photography. One interpretation of the physical significance of a linear unwrapped length vs. time, or constant unwrapping velocity, curve is that the absence of accelerations indicates that inertia effects (ribbon density, for example) are not significant. The data of Fig. 2 are discussed further in Section 4.3 of this report.

The data provided in Ref. 1 are of great importance, having been obtained by high speed spinner tests using XM579 housings and with some of the identical aluminum ribbons (.004 inch or .102 mm thick, 22.5 inches or 572mm long) used in this program. The great majority of the tests were run with aluminum ribbons with thicknesses from .003

FIG. 2   FIRING TEST DATA FOR BRASS RIBBONS, T362 FUZE

Tevelow, F.L. "Terminal Report - T362
Octopus Fuze" DOFL Report TR-673
10 August 1959

Four 1/16" Alum. Plates as Target.   All Others Impacted
on $\frac{3}{4}$" Alum. Targets

No. Coils Initially	Hub. Dia.	Ribbon Width	Ribbon Length
15	.147"	.200"	9"
13	.135"	.125"	8"
11	"	"	6"
9	"	"	5"

All Coils 4 Mils Thick

COILS REMAINING AFTER IMPACT

TARGET DISTANCE, FT.
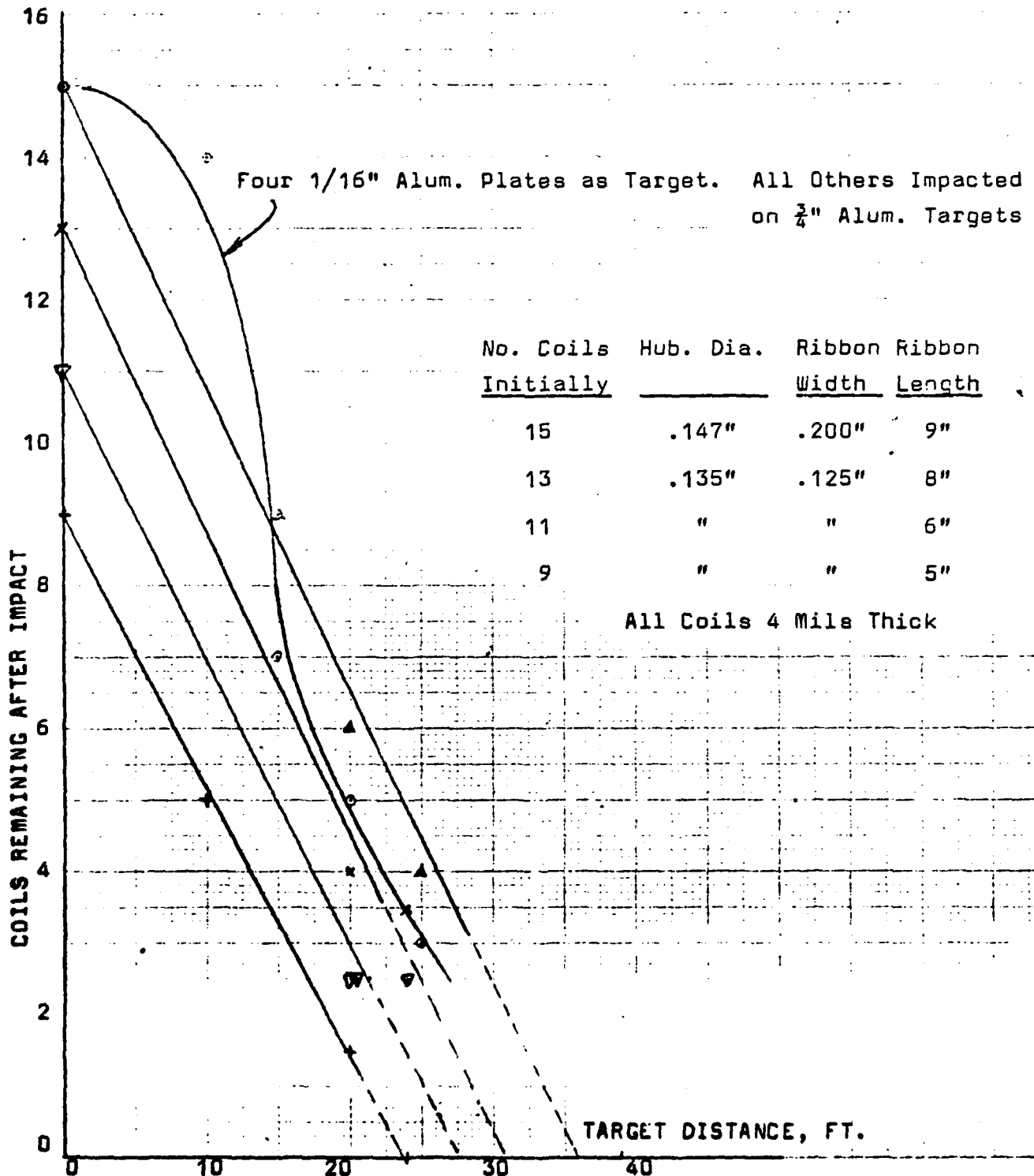
inches (.076mm) to .006 inches (.152mm), but some tests
used gilding metal ribbons with much higher density.
Despite great scatter in the data and inconsistencies
between groups of data, the following trends could be
noted:

(1) To a first approximation, neither ribbon density
nor thickness nor spin rate affected unwinding time.

(2) Unwinding time was inversely proportional to
ribbon length.

(3) The use of two .010 inch (.254mm) thick Teflon
liners between the hub and the inner coil of the ribbon
increased the unwinding time by an increment of the order
of 13 milliseconds over the unwinding time of identical
ribbons without liners.

This current program was designed to improve on the
unsystematically obtained and often conflicting data gathered
in previous programs. Ribbon dimensional and material parameters
were varied over wide ranges, as were the external inputs of
wrapping tightness and spin rate. Some of the preliminary
conclusions reached previously were confirmed and others
were refuted, as follows:

Some of the conclusions are that :—

(1) Ribbon materials had to be in a dead soft condition
to be suitable for unwinder application. Aluminum, brass,
copper and lead were found to work well, but steel and
titanium could not be annealed sufficiently to remain wound
in a coil without external restraint. Lead was used success-
fully in the laboratory test program, but it is generally
considered too soft a material to be handled in an operational
fuze application.

(2) Ribbon material properties and thickness had no

definite effect on unwinding time.

(3) Winding tightness had no definite effect on
unwinding time.

(4) Unwinding time was found to be proportional
to ribbon length divided by spin rate-times-cavity radius, *are*
as given by Equation 28 in Section 4.4.

(5) For all the empirical data gathered in this
air spinner test program, the standard deviation was 39
~~percent~~ of the mean unwinding time. This is not considered
excessive variation for an arming delay system.

Design equations for unwinding time and arming
distance are given in Section 4.4 of this report. With
the exception of corrections that may be introduced by
the setback environment or by additional forces required
to actuate specific arming mechanisms, these equations are
considered adequate for the design of practical ribbon
unwinder arming systems.

2. EXPERIMENTAL PROGRAM

2.1 Test Plan

Some of the parameters that were expected to have some influence on unwinding time of a ribbon are ribbon length and thickness and material (density, modulus of elasticity, inter-coil friction, etc.), winding tension spin rate, hub radius, and cavity radius. The latter parameters were held constant at .136 inches (3.45mm) .342 inches (8.69mm), respectively, since XM579 hardwa was adapted for use in the test spinner, and the other parameters were varied within the following limits:

Ribbon length: 10-30 inches (254-762mm)

Ribbon thickness: .0012-.004 inches (.0305-.102mm)

Materials: Aluminum, beryllium-copper, brass, copper, lead.

Winding tension: 20-570 grams

Spin rate: 20,000-33,000 rpm

An excessive number of tests would have been required to isolate the effects of variations in each parameter while all other parameters are held constant. Instead, a randomized-value test plan was designed, as described in Section 3. With this plan of approximately seventy tests (see Table 1), it is possible to determine the influence of each parameter, using a multivariate regression analysis of the data.

2.2 Ribbon Unwinder Assembly

A ribbon unwinder assembly consists of a two-piece

or split hub around which is wrapped a number of turns
of a thin metal foil. See Fig. 3 below.

a - Split Hub

b - Ribbon

c - Finished Assembly
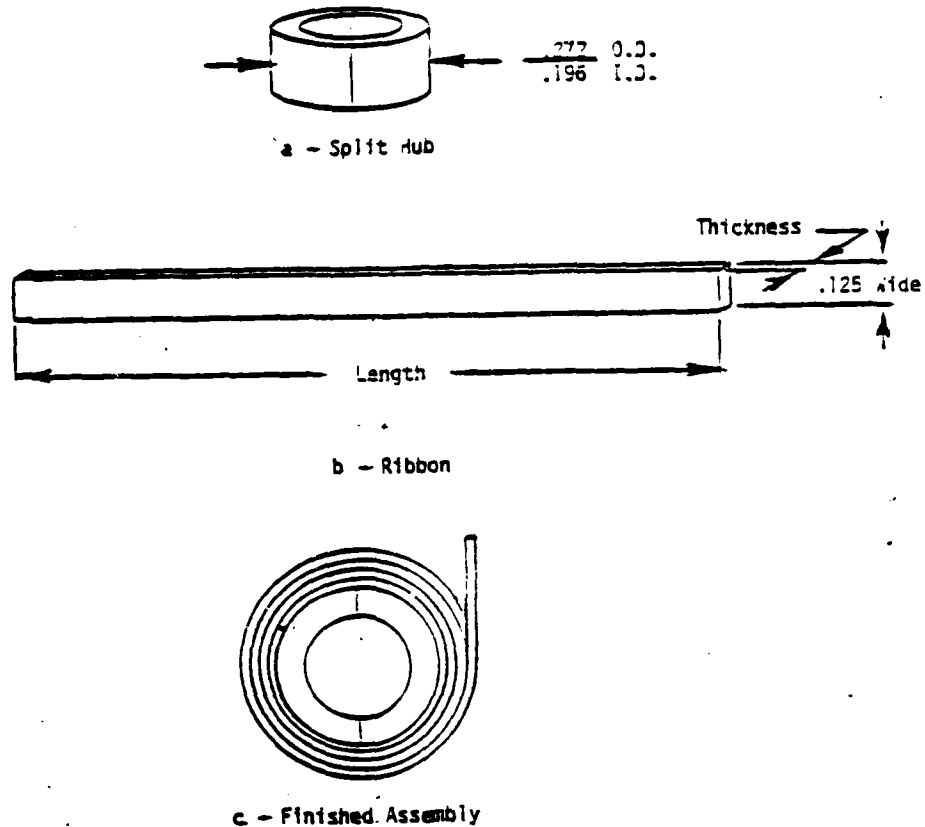
FIG. 3 RIBBON UNWINDER ASSEMBLY

The tape or ribbon of all unwinder assemblies was
.125 inches (3.18mm) wide. The length and thickness of
the tape was varied as shown in Table 1. Ribbon unwinder
assemblies were fabricated in the laboratory using a simple
hand crank mechanism to wind the ribbon onto the split hub.
See Fig. 4.
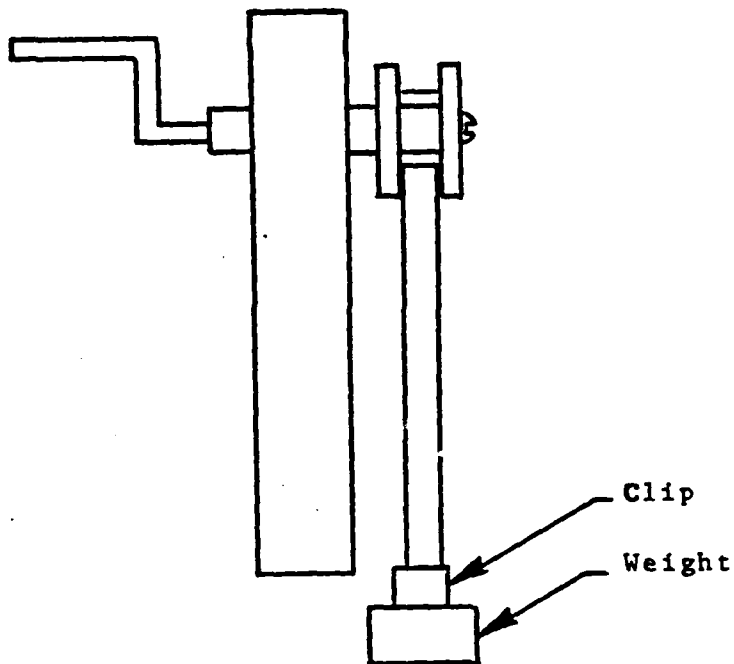
FIG. 4   HAND CRANK WINDING MECHANISM

Tension was maintained on the ribbon by means of a
weight attached to its free end. It was necessary to apply
a thin coat of magnesium oxide (milk of magnesia) to one
side of all ribbons made from aluminum, beryllium copper,
copper and brass. The magnesium oxide was applied by means
of a cotton swab during the winding operation and was needed
to prevent adjacent layers of the ribbon from sticking to
one another during the annealing process. Ribbon assemblies
made from the aforementioned materials were annealed in
the wound condition by encasing each one individually in
a special stainless steel form. Ribbon assemblies using
lead or aluminum 1100-0 did not require annealing as they
were soft enough to hold form in the as-wound condition.

Aluminum 1100-0 ribbons were obtained from fifty inert XM579 fuzes supplied to Hamilton Technology, Inc. (HTI) at the beginning of the program. HTI discovered that it was possible to rewind and retest a 1100-0 ribbon several times without degrading its timing characteristics. The aluminum ribbons were relatively easy to rewind, due to the dead soft condition of the aluminum.

Attempts were made to anneal steel and titanium ribbons, but they would not remain wound on the unwinder assembly. Accordingly, these materials were not employed in the test program.

2.3 Spinner Construction and Operation

Figure 5 shows a cutaway view of the laboratory spinner which was built at Hamilton Technology and which was used to obtain the experimental data. The high speed spinner is powered by a miniature air driven motor with speed controlled by regulated air pressure. An on-off air toggle switch is connected into the air inlet line to provide for additional air control. The air driven motor is coupled to the spinner on a one-to-one basis and the speed of the system is monitored by a Hewlett-Packard Model 5300A measuring system to which is fed signals from the light-photocell assembly at the aft end of the air motor.

Figure 5a shows the spinner without a ribbon unwinder assembly. Figure 5b shows the spinner with a ribbon unwinder assembly in place with the retainer screwed down on top of the split hub of the unwinder assembly. Figure 5c shows the spinner with the ribbon completely unwound and the two halves of the split hub thown clear of the main control shaft.
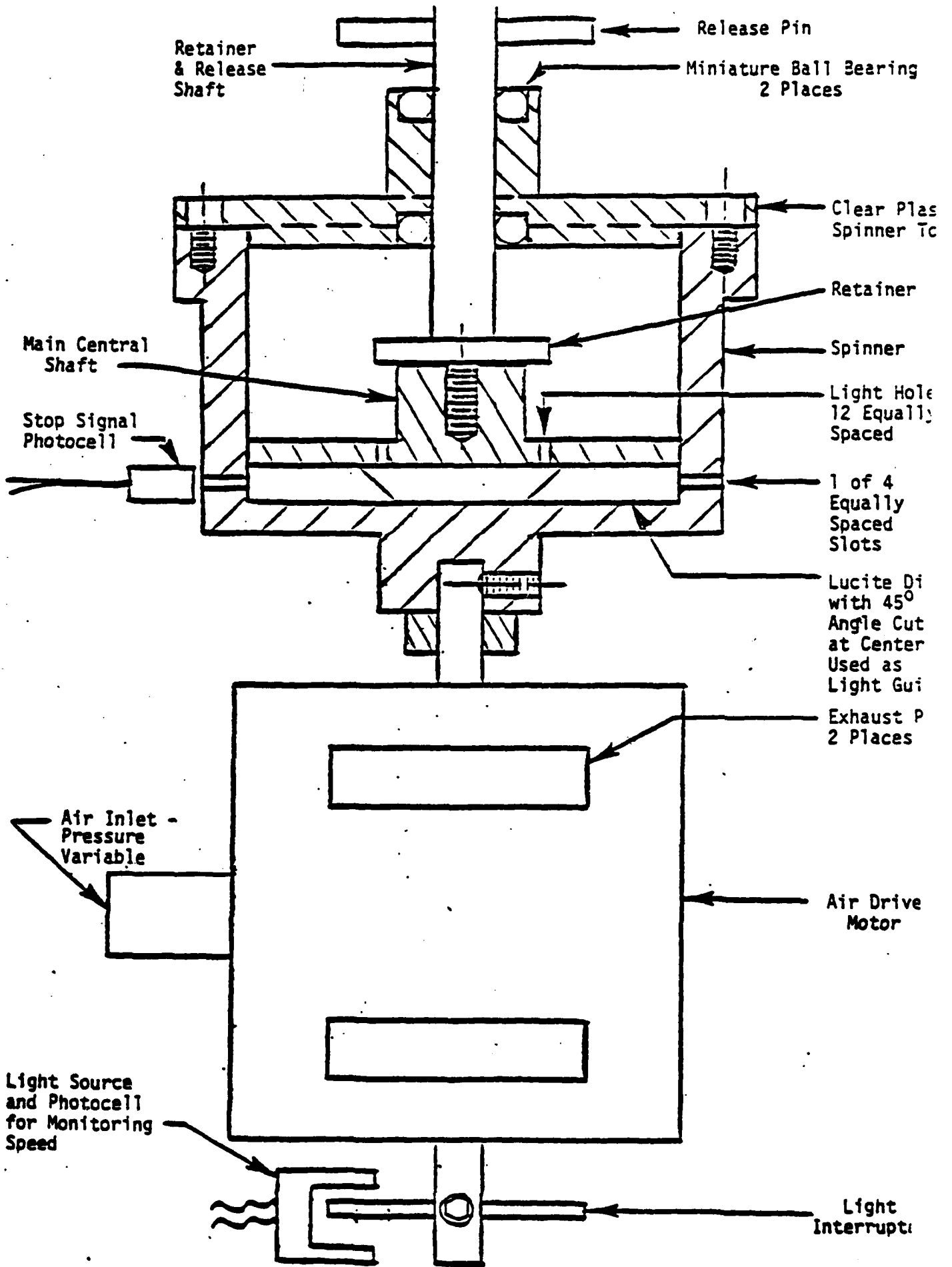
Release Pin

Retainer & Release Shaft

Miniature Ball Bearing 2 Places

Clear Plas Spinner Tc

Retainer

Main Central Shaft

Spinner

Light Hole 12 Equall; Spaced

Stop Signal Photocell

1 of 4 Equally Spaced Slots

Lucite Di with 45° Angle Cut at Center Used as Light Gui

Exhaust P 2 Places

Air Inlet - Pressure Variable

Air Drive Motor

Light Source and Photocell for Monitoring Speed

Light Interrupt

FIGURE 5a   - 13 -
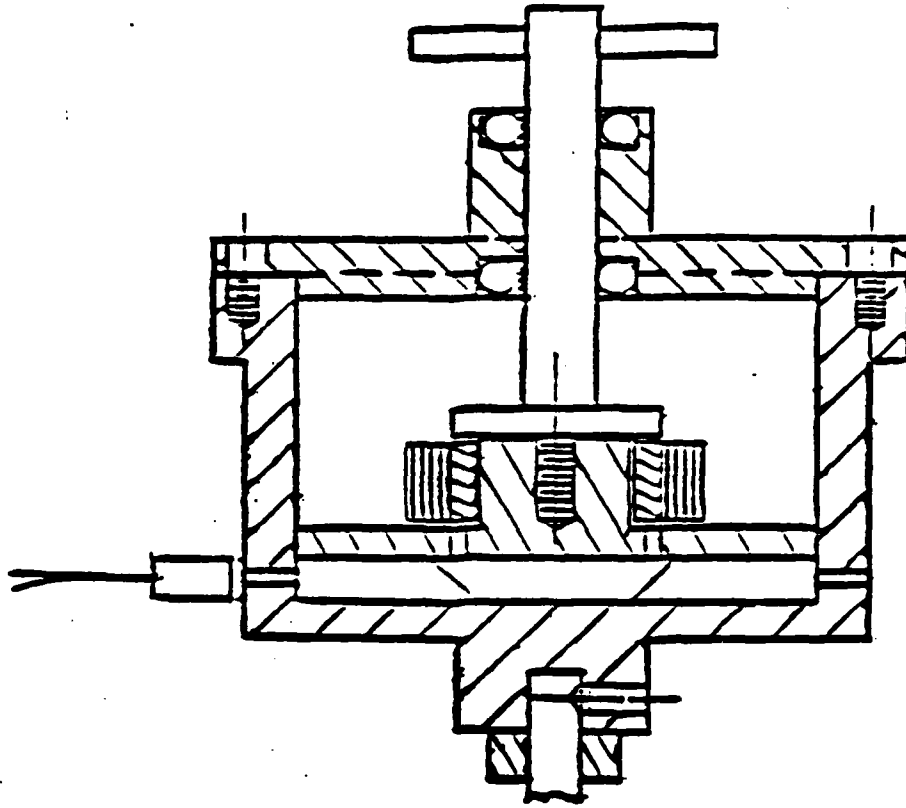
Figure 5b

Figure 5c

- 14 -
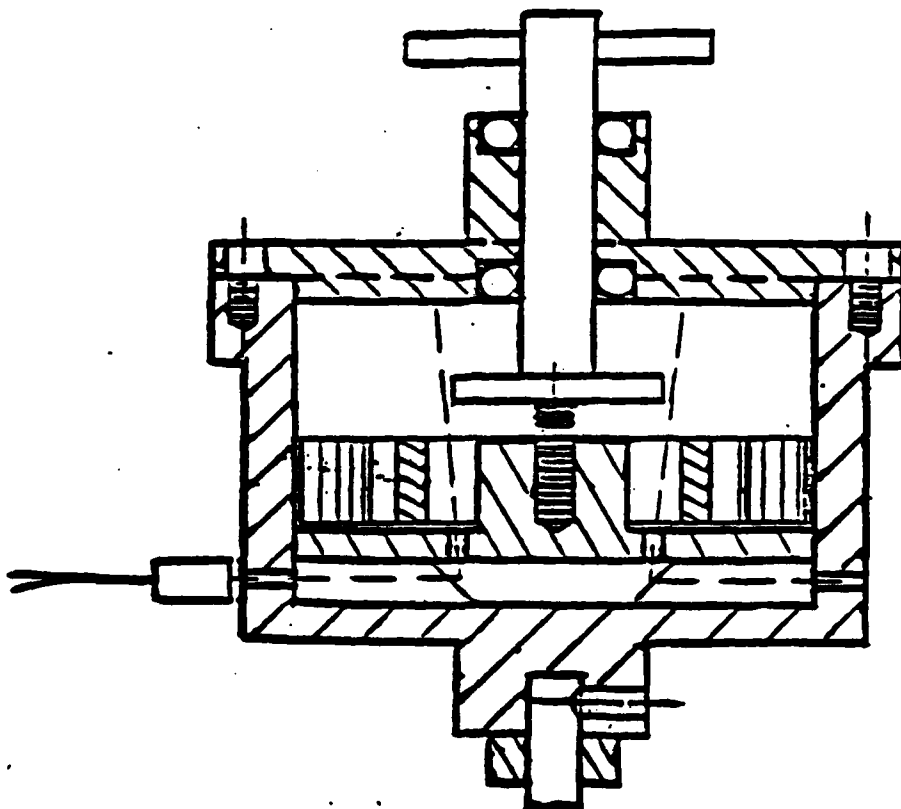
With the ribbon unwinder in place in the spinner, as shown in Fig. 5b, the air motor is accelerated until the desired speed is obtained. At this time, a mechanical interrupter, not shown, contacts the tip of the release pin causing the retainer and release shaft to move counter-clockwise, which is opposite to the clockwise spin of the spinner. At the same time, the retainer backs off from the split hub and a start signal is sent to an electronic timer. Once the split hub has been freed of the pressure of the retainer, the entire ribbon unwinder assembly starts to rotate around the main central shaft of the spinner until all of the ribbon unwinds as shown in Fig. 5c.

In the absence of friction between the ribbon and the cavity wall onto which it is being transferred, it is possible for unwinding to occur even if the hub is not allowed to rotate. This form of unwinding can occur if the free end of the coil can slide freely inside the cavity wall, allowing the point of tangency with the hub to change. In actual operation, only a small amount of ribbon was transferred to the cavity wall before friction prevented further unwrapping. In four tests of aluminum ribbons at 25,900-33,900 rpm, the number of loops trans-ferred to the cavity wall before hub release varied between $\frac{3}{4}$ and 2. Since these pre-release loops represent only a small fraction of the many loops to be transferred, this method of releasing the coil was considered accurate enough.

During the test, a concentrated beam of light is focused on the top of the spinner. This beam of light passes through the clear plastic spinner top and is blocked from further travel to the stop-signal photocell

- 15 -

by the split hub of the ribbon unwinder assembly.
However, once the ribbon has completely unwound and
the two halves of the split hub spin away from the main
central shaft, the light proceeds along a path shown by
the dotted line in Fig. 5c. When light hits the stop-
signal photocell, a stop signal is transmitted to the
electronic timer. The time between the start and stop
signals to the electronic timer is the time delay of the
ribbon unwinder.

2.4   Test Results and Data

Table 1 contains the test data obtained with the
air spinner.

In addition to the unwinding times recorded in Table
1, several ribbons were observed with high speed photography
as they unwound. Fig. 6 shows the results of a frame-by-
frame analysis of the films. Resolution was not adequate
to count the .004 inch (.102mm) thick coils; instead, the
thickness of the ribbon bundle remaining on the split ring
was measured. Several important observations may be made:

(1)   The unwinding process is fairly linear, which
implies that ribbon length is transferred at approximately
a constant velocity during unwinding.

(2)   There may be some time delay as the split ring
pushes on the innermost ribbon coil, until its final release.

(3)   The curve for Ribbon No. 2, wound in the wrong*
direction(in the direction of rotation), shows a distinctly

---

* .In Ref. 1, it is emphasized that ribbons wound in this
  way can be expected to produce unreliable results.

NO.	MATERIAL	THICKNESS INCHES	LENGTH INCHES	TENSION GRAMS	SPINNER RPM	TIME MILLISEC'S.	REMARKS
3/11/82							
1.	Alum. 1100-0	.004	22½	As rec'd.	25,906	41.5	
2.	"	"	"	"	30,000	20.9	
3.	"	"	"	"	33,708	50.5	
4.	"	"	"	"	33,898	36.8	
5.	BeCu, 25	.002	17	340	30,000	29.8	
6.	"	"	21	310	30,000	34.8	
7.	"	"	27	380	30,000	50.7	
8.	Brass, 70/30	.002	24	380	30,000	44.8	
9.	Alum. 1100-0	.004	22½	180	34,286	27.3	
10.	"	"	"	"	33,333	35.2	
3/16/82							
11.	Alum. 1100-0	.004	22½	180	25,000	-	Partially unwrapped
12.	"	"	"	"	30,000	31.8	
13.	"	"	"	"	33,776	15.0	
14.	"	"	"	"	25,000	34.0	
15.	"	"	"	"	33,333	36.4	
16.	Lead	.0025	15	80	30,612	22.7	
17.	"	.0012	28	20	30,000	42.1	
18.	Aluminum	.002	30	250	30,303	53.7	
19.	Brass, 70/30	.004	26	570	30,000	33.8	
20.	Cu, OFHC	.0015	22	280	30,612	59.5	
21.	"	"	16	380	33,784	40.2	
22.	Aluminum, 1145	.0012	23	280	30,000	-	Partially unwrapped
23.	"	"	22	340	33,708	-	"

TABLE 1   TEST DATA

- 17 -

NO.	MATERIAL	THICKNESS INCHES	LENGTH INCHES	TENSION GRAMS	SPINNER RPM	TIME MILLISEC'S.	REMARKS
4/5/82							
24.	Alum. 1100-0	.004	22½	180	30,000	33.1	
25.	Lead	.002	27	80	26,000	3.6	Time appears questionable
26.	Aluminum, 1145	.0012	13	140	33,000	-	Only 4" unwrapped
27.	"	"	28	140	29,000	-	Only 13½" unwrapped
28.	Alum. 1100-0	.004	12	180	27,000	22.2	
29.	BeCu, 25	.002	17	340	33,000	34.1	
30.	Lead	.002	21	80	31,600	51.7	
31.	Alum. 1100-0	.004	17	180	20,000	39.2	
32.	"	"	22½	180	27,000	37.7	
33.	Lead	.002	14	80	22,000	9.8	Time appears questionable
34.	Brass, 70/30	.002	39	250	30,000	63.5	
35.	Aluminum, 1145	.0012	18	140	33,000	-	Only 13" unwrapped
36.	"	"	31	140	29,000	-	Only 14½" unwrapped
37.	Alum. 1100-0	.004	22½	140	30,000	29.8	
5/10/82							
38.	BeCu, 25	.002	22	240	-	-	Unwound prematurely
39.	Cu, OFHC	.0015	18	450	20,000	-	Did not unwind
40.	Brass, 70/30	.004	12	490	-	-	Unwound prematurely
41.	"	"	27	300	31,100	35.7	
42.	"	"	14	260	24,000	29.5	
43.	"	"	12	440	26,000	33.7	
44.	BeCu, 25	.002	10	500	-	-	Unwound prematurely
45.	Brass, 70/30	.002	30	230	28,000	149.6	
46.	Cu, OFHC	.0015	14	150	30,000	53.1	
47.	BeCu, 25	.002	21	270	29,000	23.0	
48.	Brass, 70/30	.004	11	180	28,000	19.9	
49.	Brass "	.004	23	320	26,000	29.7	
50.	Cu, OFHC	.0015	30	490	25,000	108.1	
51.	Brass, 70/30	.004	26	240	21,000	39.9	
52.	"	"	15	430	31,000	30.5	
53.	"	"	19	340	30,000	47.4	
54.	BeCu, 25	.002	23	260	31,900	30.2	
55.	"	"	29	360	-	-	Unwound prematurely

TABLE 1   TEST DATA

NO.	MATERIAL	THICKNESS INCHES	LENGTH INCHES	TENSION GRAMS	SPINNER RPM	TIME MILLISEC'S.	REMARKS
5/10/82							
56.	Alum. 1100-0	.004	10	200	25,000	22.1	
57.	"	"	15	180	30,000	19.4	
58.	Brass, 70/30	"	27	300	31,600	45.9	
59.	"	"	27	300	31,600	35.0	
60.	"	.002	30	230	28,000	75.5	
61.	BeCu, 25	.002	29	360	24,000	39.2	
62.	Cu, OFHC	.0015	16½	450	25,000	54.3	Unit No. 39 with 1½" remove
63.	Alum. 1100-0	.004	22½	180	30,000	32.2	
64.	"	"	"	"	30,000	38.1	
65.	"	"	16	"	25,000	34.5	
66.	"	"	"	"	20,000	51.0	
67.	"	"	"	"	18,000	60.0	
68.	"	"	"	"	17,000	62.9	
69.	"	"	"	"	15,000	-	Partially unwrapped
70.	"	"	22½	"	32,400	24.8	

TABLE 1   TEST DATA

FIG. 6 UNWINDING RATE MEASURED FROM HIGH SPEED FILMS

.004 Aluminum, 22½" Long, Approx. 25,000 RPM

Film Speed Approx. 5,000 Frames/Sec.

° Ribbon No. 2 Wound in Direction of Rotation

° Ribbons 1,3,4 Wound Opposite to Direction of Rotation
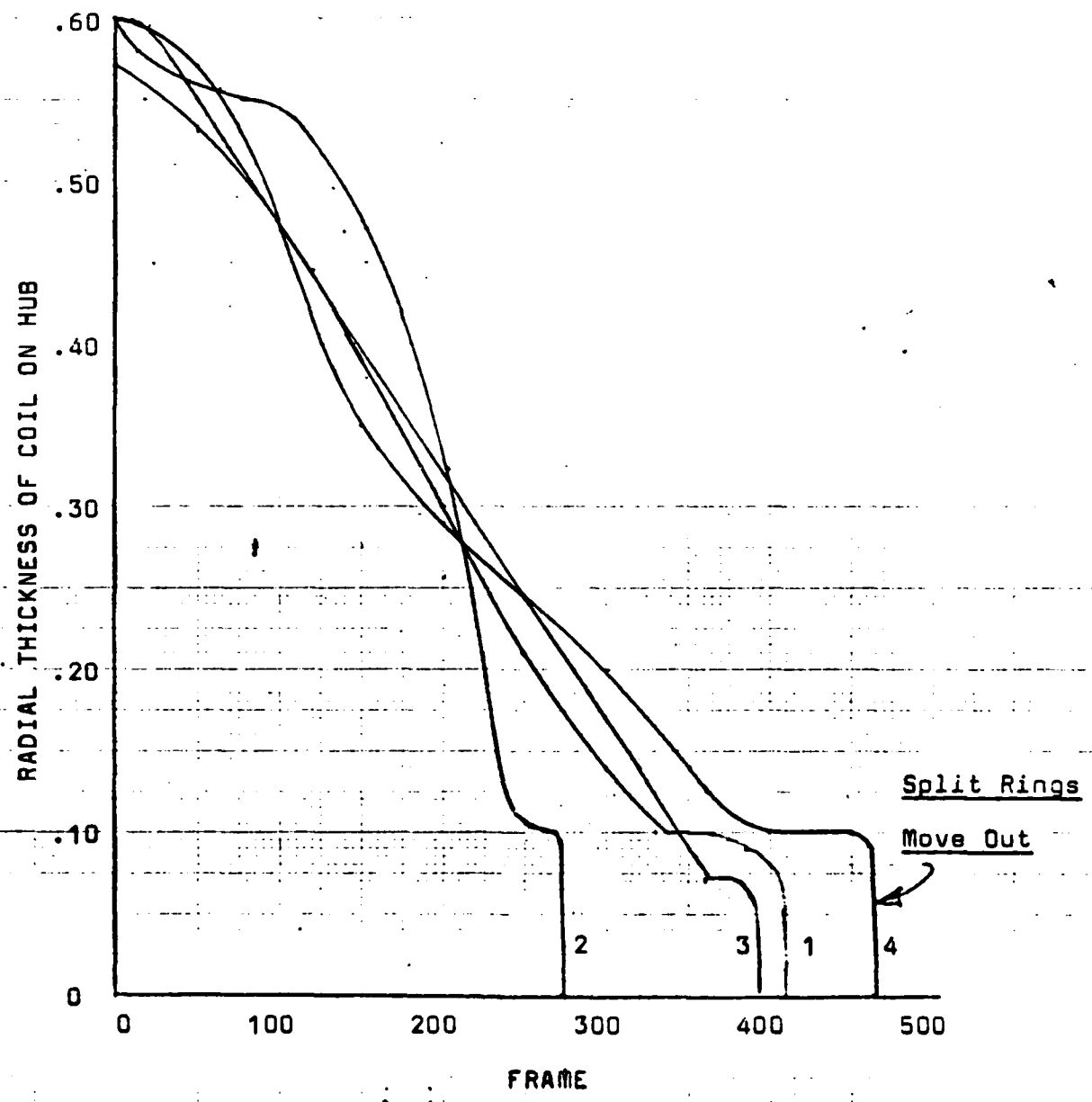
different unwinding history. The films of this event showed many coils existing in the space between the hub and the outer cavity. In contrast, the other ribbons showed only one coil at a time being transferred to the outer cavity wall.

(4) The shape of the bridge was a flat spiral, with no noticeable changes in shape as unwinding proceeded.

The observations made above were used as justification for the pseudo-stationary models developed in Section 4 of this report.

None of the six assemblies using .0012 inch (.0305mm) thick aluminum unwrapped completely, although three of the assemblies were spun at 33,000 rpm. Evidently there is not sufficient force generated at the free end of such a thin ribbon to sustain the unwrapping function.

To comment on the relative advantages of the materials used in the test program, it appears that the selection of 1100-0 aluminum for the ribbon unwinder assemblies used in the XM579 fuze was a good selection. It is inexpensive, relatively easy to wind, and does not require annealing.

3. MULTIVARIATE REGRESSION ANALYSIS BY ALN METHOD

3.1 Discussion of the Data

The objective of the work presented in this report was to obtain an empirical model that relates the ribbon unwinding time to the experimental and material-dependent parameters. The method for obtaining this model was the application of the Adaptive Learning Network (ALN) method to data collected for the present study, as well as data collected in other tests.

The ALN method is an empirically-based modeling procedure. This procedure is presented in detail in Appendix A. The advantage of this technique is the ability to obtain highly nonlinear and multidimensional models. It should be noted, however, that only that model complexity supported by the data is obtained. The ALN method does not force nonlinearity or multidimensionality into the models.

The data obtained for the present study were obtained using a spinner setup. That is, a ribbon was wound around the hub of a shell, the shell spun, and the time required for the ribbon to unwind measured. The factors that were varied were the material the ribbon was made of, its length, thickness, the spin rate, and the winding tension. The ribbons were constructed of five different materials: aluminum, beryllium-copper, brass, lead, and copper. The lengths of the ribbons varied from 10 to 30 inches, and their thicknesses varies from 1.2 to 4 mils. The winding loads were varied from 20.2 to 570 grams, and the spin rates varies from 15,000 to 33,898 rpm. A complete list of the data obtained for this study has been presented in Table 1.

Data similar in nature to the present data have been obtained in other spinner and firing tests(Ref.1,2). See Table 2.

TABLE 2   RIBBON UNWINDING DATA FROM OTHER TESTS

TEST	CONDITION	LINER THICK.	R IR.	R I?.	MATL.	n in.	L in.	RPM	NO. TESTS	MEAN MS	SIGMA
Bulova	70°F	.020	.335	.100	Alum.	.004	24	34,500	1	50	
Spinner	"	"	"	"	"	"	"	"	1	60	
	160°F	"	"	"	"	"	"	"	1	52	
	"	"	"	"	"	"	"	"	1	53	
	"	"	"	"	"	"	"	"	1	46	
	-10°F	"	"	"	"	"	"	"	1	50	
Frost {	-35/-20°F	"	"	"	"	"	"	"	1	100	
	"	"	"	"	"	"	"	"	1	74	
	70°F	"	"	"	"	"	"	29,000	6	48.6	1.1
	"	"	"	"	"	"	"	34,000	24	54.3	8.3
	"	"	"	"	"	"	"	36,000	9	46.6	7.0
	"	-	"	.125	"	.006	5	34,000	1	6	
	"	-	"	"	"	"	5	"	1	6	
	"	-	"	.0625	G.M.	.003	10	"	1	12	
	"	-	"	"	"	"	10	"	1	11	
	"	-	"	"	Al+GM	.013	6	"	1	7	
	"	-	"	.100	Alum.	.005	11	"	1	14	
	"	-	"	"	"	"	11	"	1	15	
	"	-	"	"	"	"	11	"	1	16	
	"	-	"	"	G.M.	"	11	"	1	15	
	"	-	"	"	"	"	11	"	1	14	
	"	-	"	"	"	"	11	"	1	14	
	"	-	"	"	Alum.	.004	24	"	1	37	
	"	-	"	"	"	"	"	"	1	37	
	"	-	"	"	"	"	"	"	1	31	
	"	-	"	"	G.M.	.003	11	"	1	15	
	"	.020	"	"	Alum.	.004	12	"	11	27	8
	"	.015	"	"	"	"	15	"	9	39	13
	"	.020	"	"	"	"	24	"	11	41	5
	"	.030	"	"	"	"	24	"	7	51	10
	"	.020	"	"	"	"	25	"	9	66	15
	"	.020	"	"	"	"	24	"	7	50	14
	"	.020	"	"	"	"	24	"	10	42	3
20mm	"	-	.217	.074	Brass	"	9	75,000	1	10.9	
Firings	"	-	"	.068	"	"	8	"	1	9.4	
	"	-	"	.068	"	"	6	"	1	8.3	
	"	-	"	.068	"	"	5	"	1	7.1	

Review of the data in Tables 1 and 2 reveals a number of interesting factors. First, the data in Table 1 shows there were a number of experimental trials where the ribbon did not unwind completely but where, in other trials under identical or near-identical conditions, the ribbon did unwind completely. For example, trials 11 and 14 in Table 1 represent such a case. The second observation is that the data demonstrate a certain variability, the lack of unwinding completely when they should and nearly identical trials having times varying by a factor of two (eg. trials 10 and 13). A third observation has to do with the relationship between spin rate and unwinding time. Figure 7 displays a plot of the unwinding time vs. spin rate for trials involving aluminum of 4-mil thickness and 22.5 inches length. A decrease in the unwinding time with increasing spin rate is indicated but the variance of the data is large enough to be consistent with no dependence of one on the other. (The line shown results from a least squares fit to the data). These observations are an indication that there are experimental difficulties with obtaining reproducible results.

Experimental measurements made under "identical" conditions exhibit variability in their values due to random fluctuations in the experimental process. The data in Table 2, taken from other spinner and firing tests, demonstrate variability (for the spinner data) that is inconsistent with random fluctuations. The data listed on lines 10 and 29 were nominally taken under identical experimental conditions. The first gave a mean time of 54.8 ms with a standard deviation of 8.3 ms for 24 measurements. The second resulted in a mean time of 41 ms with a 5 ms standard deviation for 11 measurements. These two sets of measurements can be tested to determine if the measured differences resulted from random fluctuations. The "T"
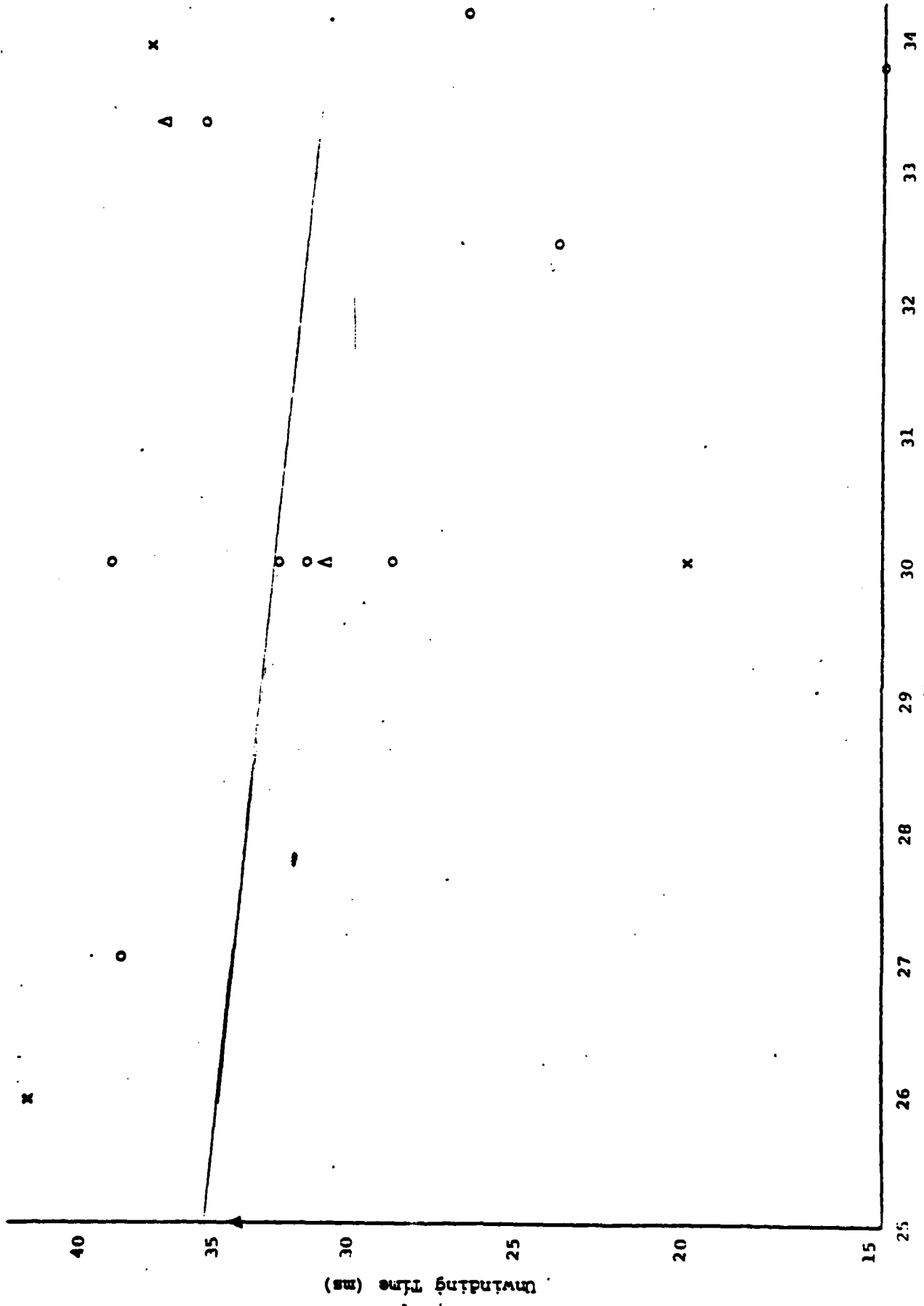
FIGURE 7   UNWINDING TIME VS. RPM

- 25 -

statistic for testing the equality of the means of two
samples is used (Ref.5):

$$T = \frac{(\cdot\frac{nm}{n+m})^{\frac{1}{2}}(\bar{x}-\bar{y})}{(\frac{nS_x^2+mS_y^2}{n+m-2})^{\frac{1}{2}}} \qquad \text{Eq. (1)}$$

where $\bar{x}$ and $\bar{y}$ are the means of the two samples, S_x and S_y,
their standard deviations, and n and m the number of samples
of x and y, respectively. For the data given above, $T=4.96$.
From the tables for T distributions, the probability of
obtaining a value of T at least as large as 4,96, for
$n+m-2 = 33$ degrees of freedom, is <u>less</u> than 0.0005. The
conclusion to be drawn from this is that the different results
obtained for the two samples did not occur due to random
fluctuations, but must be due to uncontrolled or unrecorded
variables. This set of data (Table 2) is therefore of ·
questionable value for modeling purposes and was not used
in obtaining any of the results presented below.

3.2 Adaptive Learning Network Model

The ALN modeling procedure involves identifying
candidate independent variables that are used as inputs to
the model to predict the sought-after quantity, in this
case, the ribbon unwinding time. The list of candidate
features should include, ideally, all the variables that
could conceivably affect the quantity being modeled. The
values of the independent variables, aling with the values
of the quantity being modeled, are the input data to an
Adaptronics, Inc. proprietary model synthesis program.

This program considers all the candidate independent variables in different combinations and chooses that set of combinations that best (in the statistical sense) predict the dependent variable. A complete description of this process is given in Appendix A.

The independent variables for the present data included both test parameters and material-dependent parameters, and are listed in Table 3.

TABLE 3   CANDIDATE VARIABLES

Independent Variables	Symbol
1. Spinner RPM	R
2. Material Density	μ
3. Young's Modulus	Y
4. Longitudinal Wave Velocity	V_L
5. Shear Wave Velocity	V_S
6. Thickness	T
7. Length	L
8. Winding Load	W

Values of the independent variables in Table 3 are given either in Table 1 or in Table 4, below.

TABLE 4   VALUES FOR INDEPENDENT VARIABLES

Material	Density, lb/cu.in.	Young's Modulus 1000 psi	Sound Velocity, km/sec Longitudinal	Shear
Aluminum	0.097	10,300	6.3	3.1
Brass	0.300	16,000	4.4	2.1
Be-Cu	0.300	17,000	-	-
Copper	0.320	17,000	4.7	2.3
Lead	0.410	2,000	2.2	0.7

- 27 -

Using the data in Tables 1 and 4 as inputs to the
ALN model synthesizing program the following model was
obtained for predicting the unwinding time in milliseconds:

$$t = 16.096\, \bar{E} + 39.574 \qquad \text{Eq. (2)}$$

$$\bar{E} = -.00001 + .90886A + .75419B + .77141AB - .25692B^2 \qquad \text{Eq. (3)}$$

$$A = .53317/\bar{R} - .48854\bar{T} + .41874\bar{L} \qquad \text{Eq. (4)}$$

$$B = -1.80102 + 5.1832\bar{\mu} - 5.66211\bar{Y} + 4.89211\bar{\mu}\bar{Y} \qquad \text{Eq. (5)}$$

$$\text{where} \quad 1/\bar{R} = (1/R - .36016\times10^{-4})/.64743\times10^{-5} \qquad \text{Eq. (6)}$$

$$\bar{T} = (T - .3128\times10^{-2})/.10877\times10^{-2} \qquad \text{Eq. (7)}$$

$$\bar{L} = (L - 21.095)/5.8356 \qquad \text{Eq. (8)}$$

$$\bar{\mu} = (\mu - .22334)/.11044 \qquad \text{Eq. (9)}$$

$$\bar{Y} = (Y - 13,006)/4,084.3 \qquad \text{Eq. (10)}$$

The model that resulted indicates that the reciprocal
of the RPM, the thickness of the ribbon and its length all
enter linearly into the model. The density and Young's
Modulus enter nonlinearly. This model is the best one that
can be obtained using the inputs described above.

The output of the ALN model synthesizing program is
such that many "intermediate models" are also produced.
One such model that gave good results (but not as good as
the complete model presented above) was one that used A
from Eq. 4 above in place of $\bar{E}$ in Eq. 2. This second model
is presented only because it is simpler than the above model
and yet gave good results.

Table 5 lists the predicted unwinding times for the measurement where the ribbons did not unwind completely. These values were obtained using the complete model given above.

TABLE 5   PREDICTED UNWINDING TIMES FOR TRIALS WHICH DID NOT UNWI:.D

Test No.	Material	Time, ms
11	Aluminum	36.8
22	Aluminum	45.2
23	Aluminum	41.0
25	Lead	54.5
26	Aluminum	34.3
27	Aluminum	50.3
33	Lead	49.5
35	Aluminum	38.3
36	Aluminum	52.7
39	Copper	27.8
69	Aluminum	56.3

Fig. 8 shows a computer-generated plot of the difference between the predicted and observed value of the unwinding time vs. the observed value. The model is the complete model presented above. The straight line shown results from a linear least squares fit to the data. This plot shows that the synthesized model tends to predict unwinding times that are too large for small unwinding times and too small for the longer times. The small slope and the variability of the data about the line may make the data statistically consistent with zero slope. Testing this, however, would require knowledge (which is unavailable) of the experimental uncertainties.

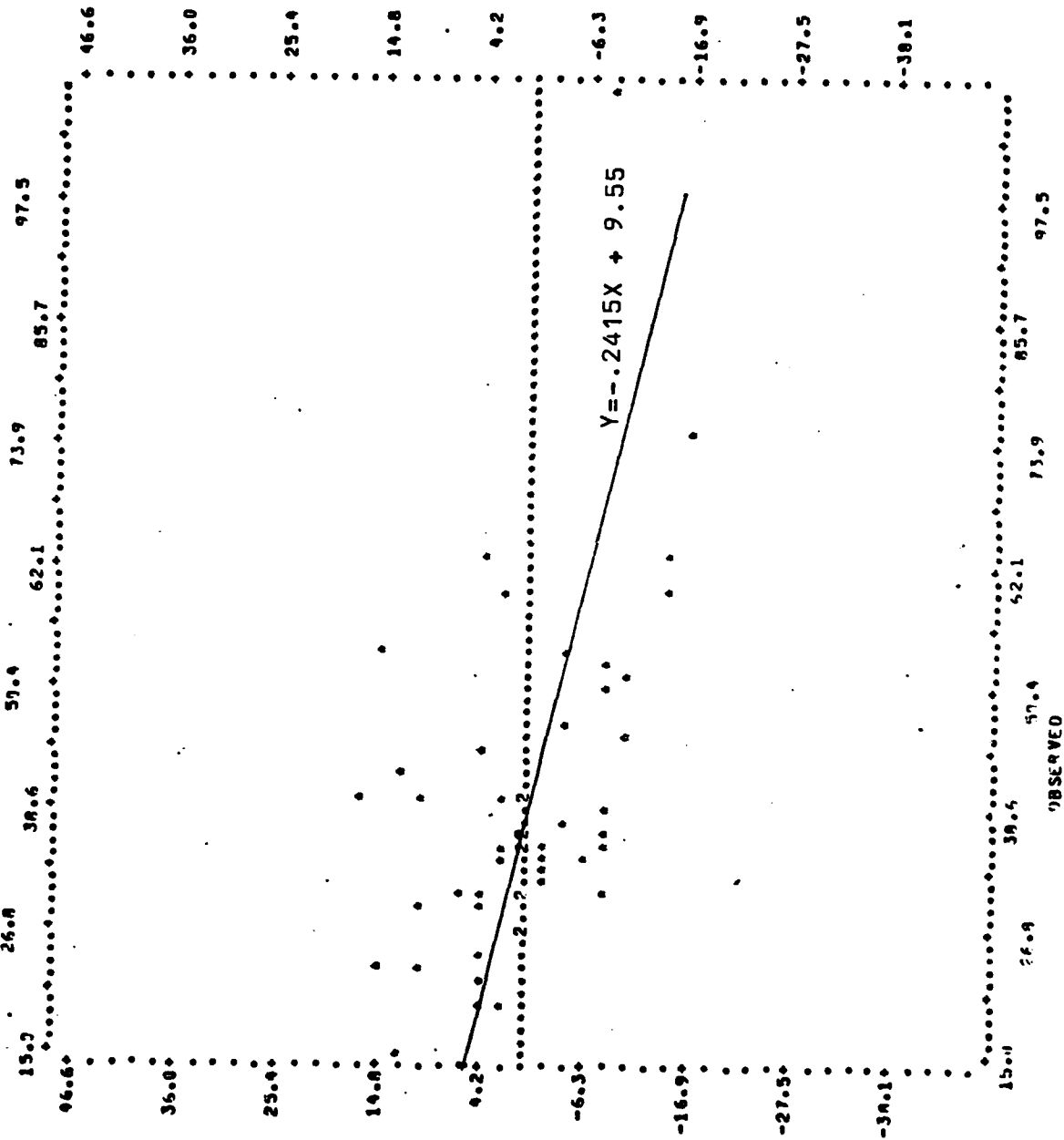FIG. 8   DIFFERENCE OF PREDICTED AND OBSERVED VALUES VS. THE OBSERVED VALUES

$Y = -.2415X + 9.55$

- 30 -

3.3 Discussion of Results

The experimental and modeling results presented above display a number of interesting features. First, the ALN model for predicting unwinding time and which resulted from fitting to the data, found that the data did not support the inclusion in the model of a "cross term" between length and reciprocal spin rate. On simple physical grounds the unwinding time of a ribbon is expected to be proportional to the length divided by the velocity of unwinding. The fact that such a term does not appear indicates only that the present data does not support its inclusion.

The second observation concerns the results in Table 5. This table presents the unwrapping time predicted by the ALN model for the experimental trials in which the ribbons did not completely unwind. The predicted unwinding times indicate that all the ribbons should have unwound completely.

The third observation concerns Fig. 8. The results in this figure suggest that there is one or more experimental factors which are not accounted for in the ALN model and which result in the model predicting too long an unwinding time for short unwinding times and too short a time for the longer times. Note that this observation is based on an _assumption_ that the observed slope to the data is statistically inconsistent with zero. If the slope is statistically consistent with zero then the results shown in Fig. 8 could have resulted from normal random fluctuations in experimental processes. In an attempt to determine if the missing factor was material-related the plot shown in Fig. 8 was redone, highlighting the different materials. No correlation with ribbon material was evident.

- 31 -

The conclusions that can be drawn from the present data analysis are the following. First, the ALN model that was obtained from fitting to the experimental data in Table 1 identified five variables as being important for predicting ribbon unwinding times. Those variables were: ribbon length, thickness, density, Young's modulus, and the reciprocal of the spin rate. Three of these (1/R, T, and L) entered into the model linearly and the other two nonlinearly.

The second conclusion is the present modeling results suggest that there is one or more unspecified experimental factors that result in the synthesized model predicting times which are too long for small unwinding times (less than 40 ms) and too short for longer unwinding times.

The third conclusion is that the present data displays a large variability. For approximately 15 percent of the experimental trials the ribbons did not unwind completely. The other data and the modeling results indicate that the ribbons should have unwound completely.

The fourth conclusion is that the data from other spinner tests, listed in Table 2, cannot be reliably used for modeling purposes. Nominally identical sets of measurements gave results which are inconsistent and could not have resulted from random fluctuations. The present analysis indicates that future work in the area of ribbon unwinders should first concentrate on determining the experimental factors involved in obtaining reproducible results.

4. ANALYTICAL MODELS OF UNWINDER DYNAMICS

4.1 The Straight Bridge Model

Fig. 9 shows two possible configurations of the bridge, or ribbon moving in the space between the coil on the hub and the coil deposited inside the cavity. The dashed ribbon shape resembles the shape observed by high speed photography, but the straight-line shape is more convenient for approximate analysis. A radial force F_p is shown inside the coil to represent the centrifugal force exerted by a pin, as in the XM579 fuze, or by the split hub segments employed in this test program. The forces on a particle with mass m moving in the rotating field with relative radial velocity V_r and relative tangential velocity V_t are as follows:

Radial force, $\quad F_r = m(\omega^2 r + V_t^2/r + 2\omega V_t)$ $\qquad$ Eq. (11)

Coriolis force, $F_c = 2m\omega V_r$ $\qquad$ Eq. (12)

If the ribbon is assumed to have no bending stiffness, the only other forces on the bridge will be cavity friction force f_c, hub friction force f_h, and inertial reactions if the hub and/or bridge mass are being accelerated.

Using Eq.11 and Eq.12, the dynamics of unwinding could be studied from the time the free end of the coil starts to unwind from the hub until the entire coil has been transferred to the cavity wall. The bridge shape (which could change throughout the unwinding process) and the motion of each ribbon particle could be calculated
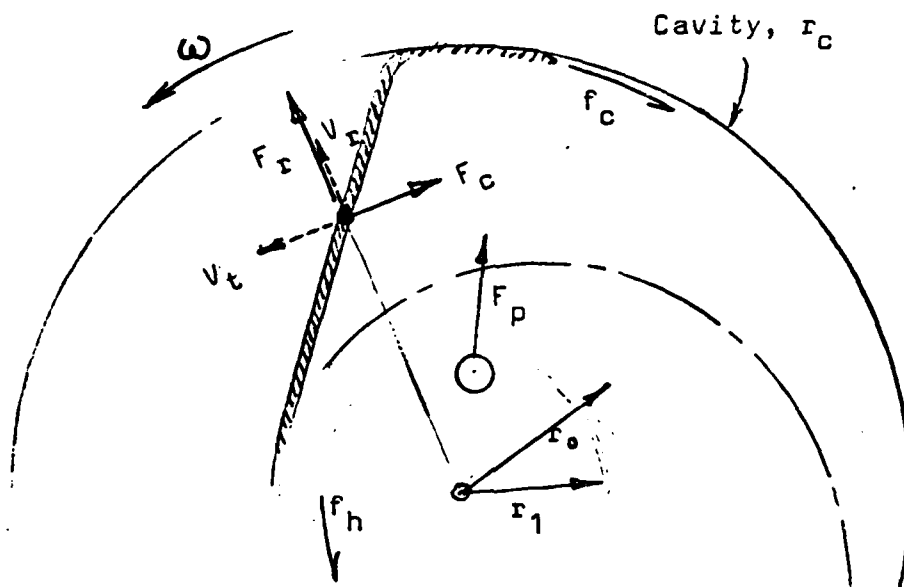
FIG. 9   RELATIVE VELOCITIES AND FORCES, STRAIGHT BRIDGE MODEL

From Eq.11, Eq.12, and Newton's laws relating forces to
changes in V_r and V_t.   Although this approach would be
extremely valuable in revealing the effects of material
density, bending stiffness and friction, it is well beyond
the scope of the present program of analysis.   Instead,
the multivariate regression analysis of experimental data
is relied upon to reveal the influence of these parameters,
and the analysis is restricted to the more approximate
approach of evaluating ribbon dynamics with an assumed
bridge shape.

     It was observed experimentally that ribbon unwinding
velocity was fairly constant, and the bridge shape remained
fairly constant, all throughout the unwinding process.
This implies a pseudo-stationary process with no acceleration

of the hub. Also, since the bridge shape is stationary
in the rotating coordinate system, there are no net
accelerations on the ribbon particles beyond those required
to maintain the bridge in that configuration. These
assumptions permit the unwinding dynamics to be analyzed
from a rather simplified viewpoint, namely, to determine
what ribbon unwinding velocity will produce centrifugal
and Coriolis accelerations that maintain the assumed
(constant) bridge shape. This approach is used to analyze
the straight bridge model (and also the standing wave model)
as follows.

Fig. 10 shows the straight bridge model with mass
concentrated at the midpoint of the bridge, in its initial
position and then after ribbon length $\theta_u r_c$ has been de-
posited on the cavity wall. The point of tangency at the
hub moves through angle θ_u. In order for the length of
the bridge to remain unchanged, the hub must rotate through
angle θ_h as follows:

$$r\theta_h + r\theta_u = r_c\theta_u$$

$$\theta_h/\theta_u = r_c/r - 1 \qquad\qquad \text{Eq. (13)}$$

The bridge's center of gravity moves from its
initial position at $AD = \frac{1}{2}(r_c^2 - r^2)^{\frac{1}{2}}$ to $BC = AD - r_c\theta_u$.
Its radial distance is now increased to $\left[r^2 + (2AD-BC)2\right]^{\frac{1}{2}} =$
$\left[\frac{3}{4}r^2 + \frac{1}{4}r_c^2 + r_c\theta_u(r_c^2 - r^2)^{\frac{1}{2}} + r_c^2\theta_u^2\right]^{\frac{1}{2}}$. For small values of θ_u
this expression reduces to $(\frac{3}{4}r^2 + \frac{1}{4}r_c^2)^{\frac{1}{2}} + \dfrac{r_c\theta_u(r_c2-r^2)^{\frac{1}{2}}}{2(\frac{3}{4}r^2 + \frac{1}{4}r_c^2)^{\frac{1}{2}}}$

The change in radial distance from its original radius of
$r_2 = \left[r^2 + \frac{1}{4}(r_c^2 - r^2)\right]^{\frac{1}{2}}$ is as follows:
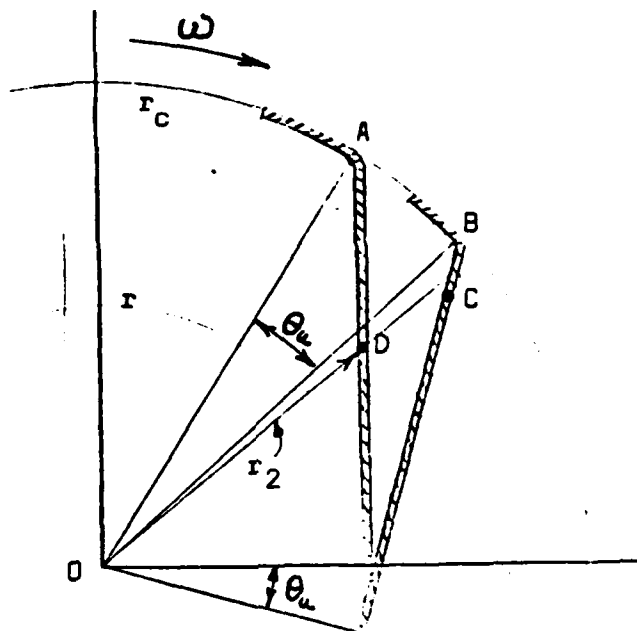
FIG. 10   MOTION OF BRIDGE WITHOUT SLIPPAGE AT CAVITY

$$\Delta r = r_c \theta_u \left(\frac{r_c^2 - r^2}{r_c^2 + 3r^2} \right)^{\frac{1}{2}}$$

$$\frac{\Delta r}{r_c \theta_u} = \left(\frac{r_c^2/r^2 - 1}{r_c^2/r^2 + 3} \right)^{\frac{1}{2}} \qquad \text{Eq. (14)}$$

The angle of rotation of the radius vector OD to OC is equal to $\tan^{-1} AD/r - \tan^{-1} \frac{2AD-BC}{r} + \theta_u$. Since $\tan^{-1} x - \tan^{-1} y = (x-y)/(1+xy)$, the angle of rotation is equal to:

$$\theta_u - \frac{r(AD - BC)}{r^2 + 2(AD)^2 - (AD)(BC)} = \theta_u - \frac{r(r_c \theta_u)}{r^2 + \frac{1}{2}(r_c^2 - r^2) - \frac{1}{2}(r_c^2 - r^2)^{\frac{1}{2}} \left[\frac{1}{2}(r_c^2 - r^2)^{\frac{1}{2}} - r_c \theta_u \right]}$$

$$\approx \theta_u \left(\frac{\frac{3}{4}r^2 + \frac{1}{4}r_c^2 - rr_c}{\frac{3}{4}r^2 + \frac{1}{4}r_c^2} \right). \quad \text{Tangential motion is obtained by}$$

- 36 -

multiplying the angular change $\Delta\theta$ by radial distance r_2:

$$r_2\,\Delta\theta = \theta_u \frac{\frac{3}{4}r^2 + \frac{1}{4}r_c^2 - rr_c}{(\frac{3}{4}r^2 + \frac{1}{4}r_c^2)^{\frac{1}{2}}} = \theta_u \frac{(r_c - r)(r_c - 3r)}{2(3r^2 + r_c^2)^{\frac{1}{2}}}$$

$$\frac{r_2\,\Delta\theta}{r_c\theta_u} = \frac{(r_c/r - 1)(r_c/r - 3)}{(2r_c/r)(3 + r_c^2/r^2)^{\frac{1}{2}}} \qquad \text{Eq. (15)}$$

Radial motion $\Delta r / r_c\theta_u$ and tangential motion $r_2\Delta\theta/r_c\theta_u$ are plotted in Fig. 11 vs. r_c/r.

Radial force F_r and tangential force (or Coriolis force) F_c are shown in Fig. 9. Tensile force T along the ribbon will be as follows:

$$T = F_r \frac{(r_c^2 - r^2)^{\frac{1}{2}}}{r(r_c^2 + 3r^2)^{\frac{1}{2}}} + F_c \frac{2r}{(r_c^2 + 3r^2)^{\frac{1}{2}}} \qquad \text{Eq. (16)}$$

where F_r and F_t are given in Eq.11 and Eq.12 in terms of radial velocity V_r and tangential velocity V_t.

The net tangential force is equal to $F_c - T\dfrac{2r}{(r_c^2 + 3r^2)^{\frac{1}{2}}}$ and it will be equal to zero if the bridge shape remains constant as the ribbon unwinds. Therefore:

$$F_c = T\frac{2r}{(r_c^2 + 3r^2)^{\frac{1}{2}}} = F_r \frac{2r(r_c^2 - r^2)^{\frac{1}{2}}}{r(r_c^2 + 3r^2)} + F_c \frac{4r^2}{(r_c^2 + 3r^2)}$$

$$F_r/F_c = \frac{r_c^2 - r^2}{2r(r_c^2 - r^2)^{\frac{1}{2}}} = \frac{1}{2}(r_c^2/r^2 - 1)^{\frac{1}{2}} = \alpha \qquad \text{Eq. (17)}$$

FIG. 11   RADIAL AND TANGENTIAL MOTIONS

RADIAL MOTION

MOTION/AMOUNT UNWOUND

CAVITY RADIUS/COIL RADIUS

TANGENTIAL MOTION
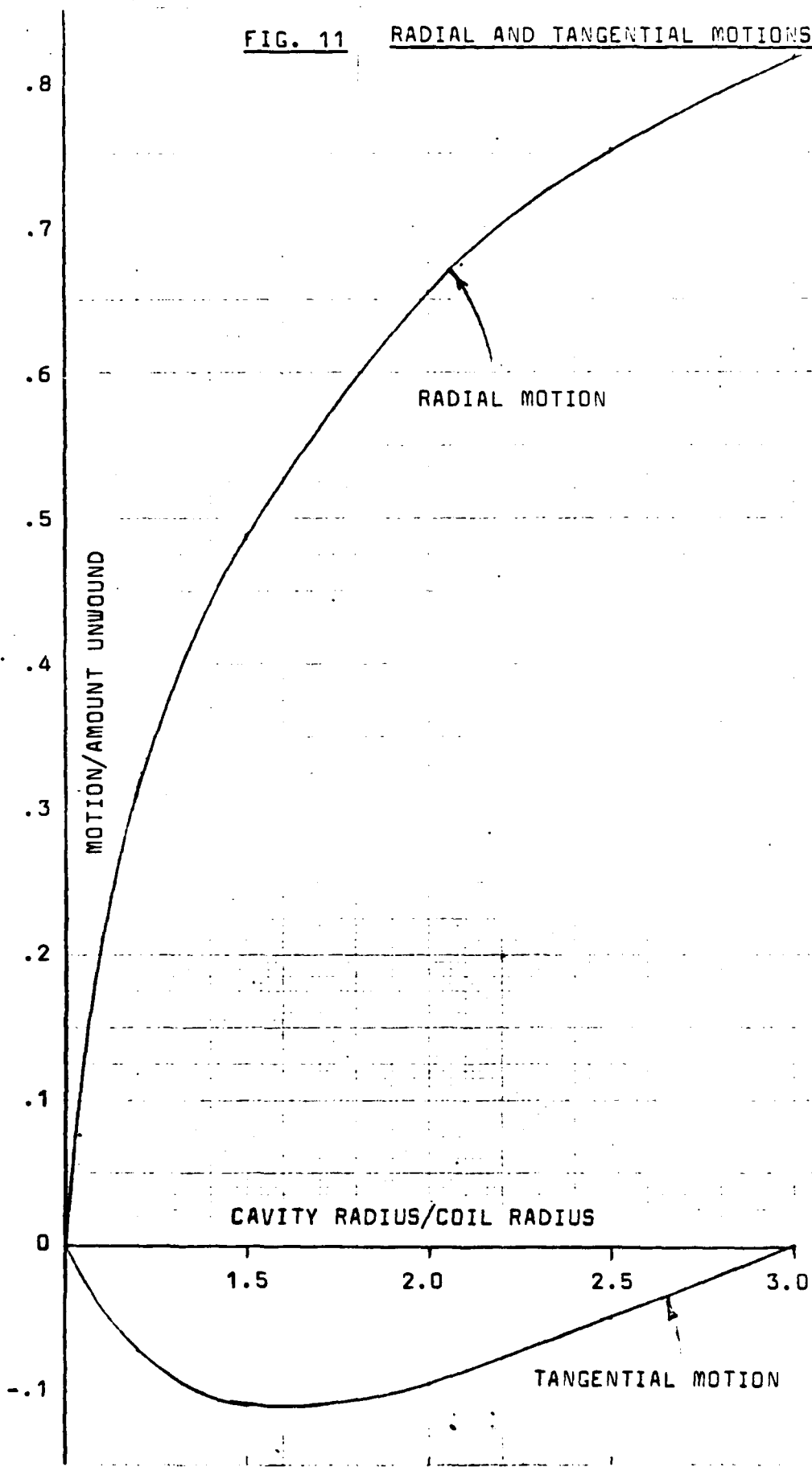
The same Eq. 17 is obtained if the net radial force is equated to zero. It is gratifying that the straight bridge model is consistent in this regard.

From Eq.11 and Eq.12:

$$F_r/F_c = \frac{\omega^2 r + V_t^2/r + 2\omega V_t}{2\omega V_r}$$

Combining this with Eq. 17:

$$2\alpha\omega V_r = \omega^2 r + V_t^2/r + 2\omega V_t \qquad \text{Eq. (18)}$$

V_t and V_r are also proportional to $r_2\Delta\theta$ and Δr, respectively. Combining these relationships with Eq. 14 and Eq.15:

$$V_r/V_t = \Delta r/r_2\Delta\theta = \frac{(2r_c/r)(r_c^2/r^2-1)^{\frac{1}{2}}}{(r_c/r -1)(r_c/r -3)} = \beta \qquad \text{Eq. (19)}$$

Combining Eq.18 and Eq.19:

$$V_t^2 + 2r\omega V_t(1-\alpha\beta) + \omega^2 r^2 = 0$$

$$2V_t = -2r\omega(1-\alpha\beta) - \left[4r^2\omega^2(1-\alpha\beta)^2 - 4\omega^2 r^2\right]^{\frac{1}{2}}$$

$$V_t/r\omega = \alpha\beta(1-2/\alpha\beta)^{\frac{1}{2}} + (1-\alpha\beta) \qquad \text{Eq. (20)}$$

where $\alpha\beta = (r_c/r)(r_c/r+1)/(r_c/r-3)$. To relate V_t to unwinding rate dL/dt, note that Eq.15 relates tangential deflection to unwound length $r_c\theta_u$. Since $r_2\Delta\theta/V_t = r_c\theta_u/\dot{L}$:

$$\dot{L}/V_t = r_c\theta_u/r_2\Delta\theta \qquad \text{Eq. (21)}$$

- 39 -

Table 6 contains values of $\alpha\beta$, $V_t/r\omega$, $V_r/r\omega$, and $\dot{L}/r$ vs. r_c/r.

r_c/r	1.0	1.2	1.5	2.0	2.5	2.9
$\alpha\beta$	-1.000	-1.467	-2.50	-6.00	-17.5	-113
$V_t/r\omega$	.268	.212	.146	.0719	.0270	.00438
$V_r/r\omega$	∞	.938	.653	.498	.413	.366
$\dot{L}/r\omega$	∞	2.94	1.34	.756	.550	.452

TABLE 6   UNWINDING RATE VS. r_c/r

Fig. 12 contains plots of V_t, V_r, and $\dot{L}$ vs. r_c/r (plus velocity V_s predicted by a standing wave model discussed in Section 4.2).

To calculate the unwinding time of any particular ribbon, $\dot{L}$ may be taken from Fig.12 for each value of r_c/r as the ribbon unwinds. For a tightly wound ribbon, it may be shown that the length L remaining on the hub is as follows:

$$L = \pi(r^2 - r_1^2)/h \qquad \text{Eq. (22)}$$

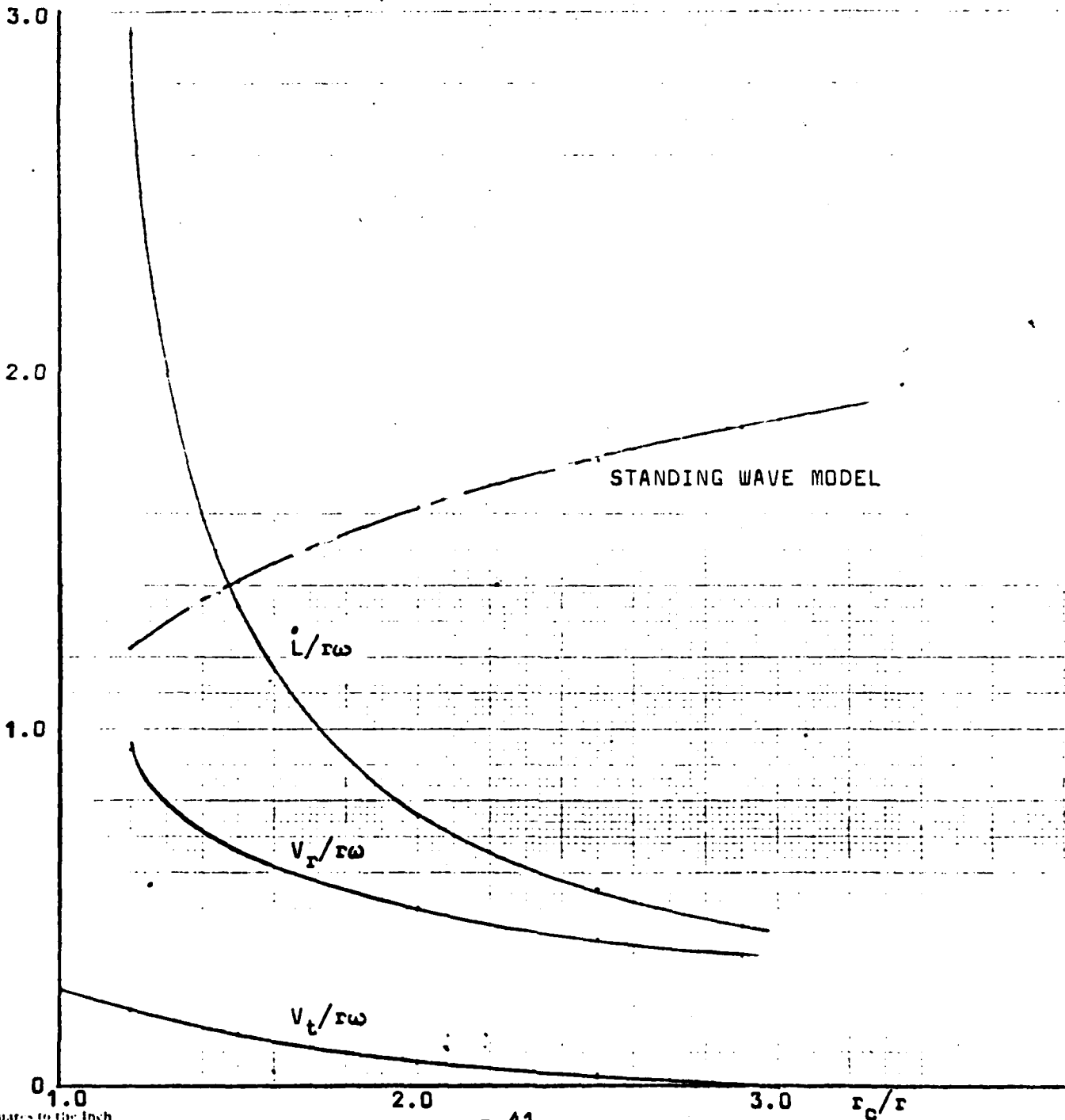where h is the ribbon thickness and r_1 is hub radius.

It may also be shown that the initial cavity radius r_{co} is reduced approximately as follows:

$$r_c = r_{co} - h(L_o - L)/2\pi r_{co} \qquad \text{Eq. (23)}$$

Combining Eq.22 and Eq.23:

- 40 -

FIG. 12   VELOCITIES IN STRAIGHT BRIDGE MODEL

STANDING WAVE MODEL

$\dot{L}/r\omega$

$V_r/r\omega$

$V_t/r\omega$

r_c/r

- 41 -

$$r_c/r = \frac{r_{co} - h(L_o - L)/2\pi r_{co}}{(hL/\pi + r_1^2)^{\frac{1}{2}}} \qquad \text{Eq. (24)}$$

A sample calculation is given in Table 7 for a 22.5 inch long aluminum ribbon with $h = .004$ inches tested at 30,000 rpm (3142 rad/sec) in the air spinner with $r_1 = .136$ inches (outer radius of the split rings) and $r_{co} = .342$ inches.

ΔL, inches	2.4	2.4	2.4	2.4	2.4	2.4	2.4	2.4	2.4	0.9
Mean L, in.	21.3	18.9	16.5	14.1	11.7	9.3	6.9	4.5	2.1	.45
r, in. (Eq.22)	.214	.206	.199	.191	.183	.174	.165	.156	.146	.138
r_c (Eq.23)	.340	.335	.331	.326	.322	.317	.313	.308	.304	.301
r_c/r	1.59	1.63	1.66	1.71	1.76	1.82	1.90	1.97	2.08	2.18
$r\omega$, in/sec.	672	648	624	600	574	547	519	489	457	434
$\dot{L}$, in/sec	793	729	674	612	554	498	431	381	327	287
$\Delta t = \frac{\Delta L}{\dot{L}}$, ms	3.03	3.29	3.56	3.92	4.33	4.82	5.57	6.29	7.35	3.14

45.3 ms

TABLE 7   UNWINDING TIME OF 22.5 INCH RIBBON

Table 8 contains calculations of unwinding times of shorter ribbons with $h = .004$ inches and the same hub and cavity dimensions.

Tables 7 and 8 show that unwinding times decrease as L_o decreases, but not nearly as much as if unwinding speed had remained constant. The 22.5 inch ribbon had an average unwinding speed of 515 in/sec, the 15 inch ribbon unwound at 397 in/sec, and the 10 inch ribbon unwound at 337 in/sec.

L_0	15.0						10.0			
ΔL	2.4	2.4	2.4	2.4	2.4	3.0	2.4	2.4	2.4	2.8
Mean L, in.	13.8	11.4	9.0	6.6	4.2	1.5	8.8	6.4	4.0	1.4
r, in.	.190	.182	.173	.164	.154	.143	.172	.163	.154	.142
r_c, in.	.340	.335	.331	.326	.322	.317	.340	.335	.331	.326
r_c/r	1.79	1.84	1.91	1.99	2.09	2.22	1.98	2.06	2.15	2.30
$r\omega$, in/sec	597	572	544	515	485	449	542	513	483	447
$\dot{L}$	557	506	446	397	344	290	420	377	327	273
t,ms	4.31	4.74	5.38	6.05	6.97	10.4	5.71	6.37	7.34	10.3
Total ms						37.8				29.7

TABLE 8   UNWINDING TIMES OF SHORTER RIBBONS

Ribbon thickness will affect unwinding time, according to the straight bridge model, by its effects on the geometry of r and r_c. To illustrate this, calculations are shown in Table 9 of 15 inch ribbons .002 inches thick and .006 inches thick (the .004 inch thickness is given in Table 8). ·

h, in.	.002						.006					
ΔL	2.4	2.4	2.4	2.4	2.4	3.0	2.4	2.4	2.4	2.4	2.4	3.0
Mean L,in	13.8	11.4	9.0	6.6	4.2	1.5	13.8	11.4	9.0	6.6	4.2	1.5
r, in.	.165	.161	.156	.151	.146	.139	.212	.201	.189	.176	.163	.146
r_c, in.	.341	.339	.336	.334	.332	.329	.339	.332	.325	.319	.312	.304
r_c/r	2.07	2.10	2.16	2.21	2.27	2.37	1.60	1.65	1.72	1.81	1.91	2.09
$r\omega$, in/sec	519	504	489	473	457	438	665	631	594	554	512	459
$\dot{L}$	374	355	329	307	286	258	778	691	600	507	422	326
t,ms	6.42	6.75	7.30	7.81	8.40	11.6	3.08	3.47	4.00	4.73	5.68	9.21
Total ms						48.3						30.2

TABLE 9   UNWINDING TIME VS. THICKNESS

Ribbon unwinding time is predicted to be a strong function of ribbon thickness, according to the straight bridge model. This effect is produced because the ribbon thickness affects the r to r_c space. However, ribbon thickness also affects ribbon stiffness, which is a factor not even considered in this model. The standing wave model discussed below, however, does contain stiffness effects.

4.2 The Standing Wave Model

A wave in a zero-stiffness string (or ribbon) moves with the following velocity:

$$V_s = (T/\rho A)^{\frac{1}{2}}$$ Eq. (25)

where T is the tensile force, ρ is density, and A is the cross-sectional area. For a straight bridge, as in Fig.9, the mass of the bridge is $\rho A (r_c^2 - r^2)^{\frac{1}{2}}$. Entering ρA into Eq.25:

$$\bullet \quad V_s = (T/m)^{\frac{1}{2}}(r_c^2 - r^2)^{\frac{1}{4}}$$ Eq. (26)

Combining Eq.26 with Eq.16 for T and Eqs.11 and 12 for F_r and F_c:

$$(V_s/r\omega)^2 = (\frac{r_c^2 - r^2}{r_c^2 + 3r^2})^{\frac{1}{2}} \left[(r_c^2/r^2 - 1)^{\frac{1}{2}}(1 + V_t/r\omega)^2 + 4V_r/r\omega \right]$$ Eq. (27)

Taking $V_t/r\omega$ and $V_r/r\omega$ from Table 6, wave velocities $V_s/r\omega$ are calculated and presented in Table 10.

- 44 -

r_c/r	1.2	1.5	2.0	2.5	2.9
$V_t/r\omega$	.212	.146	.0719	.0270	.00438
$V_r/r\omega$	.938	.653	.498	.413	.366
$V_s/r\omega$	1.220	1.411	1.615	1.750	1.842

TABLE 10   VELOCITIES IN STANDING WAVE MODEL

These standing wave velocities are plotted in Fig.12 for comparison with $\dot{L}$ predicted by the straight bridge model. At most practical values of r_c/r, the standing wave model predicts higher unwinding velocities than does the straight bridge model. For comparisons of total unwinding times, the .004 inch thick ribbons with lengths of 22.5 inches, 15 inches, and 10 inches are calculated, as shown in Table 11, under the same conditions used in Tables 7 and 8.

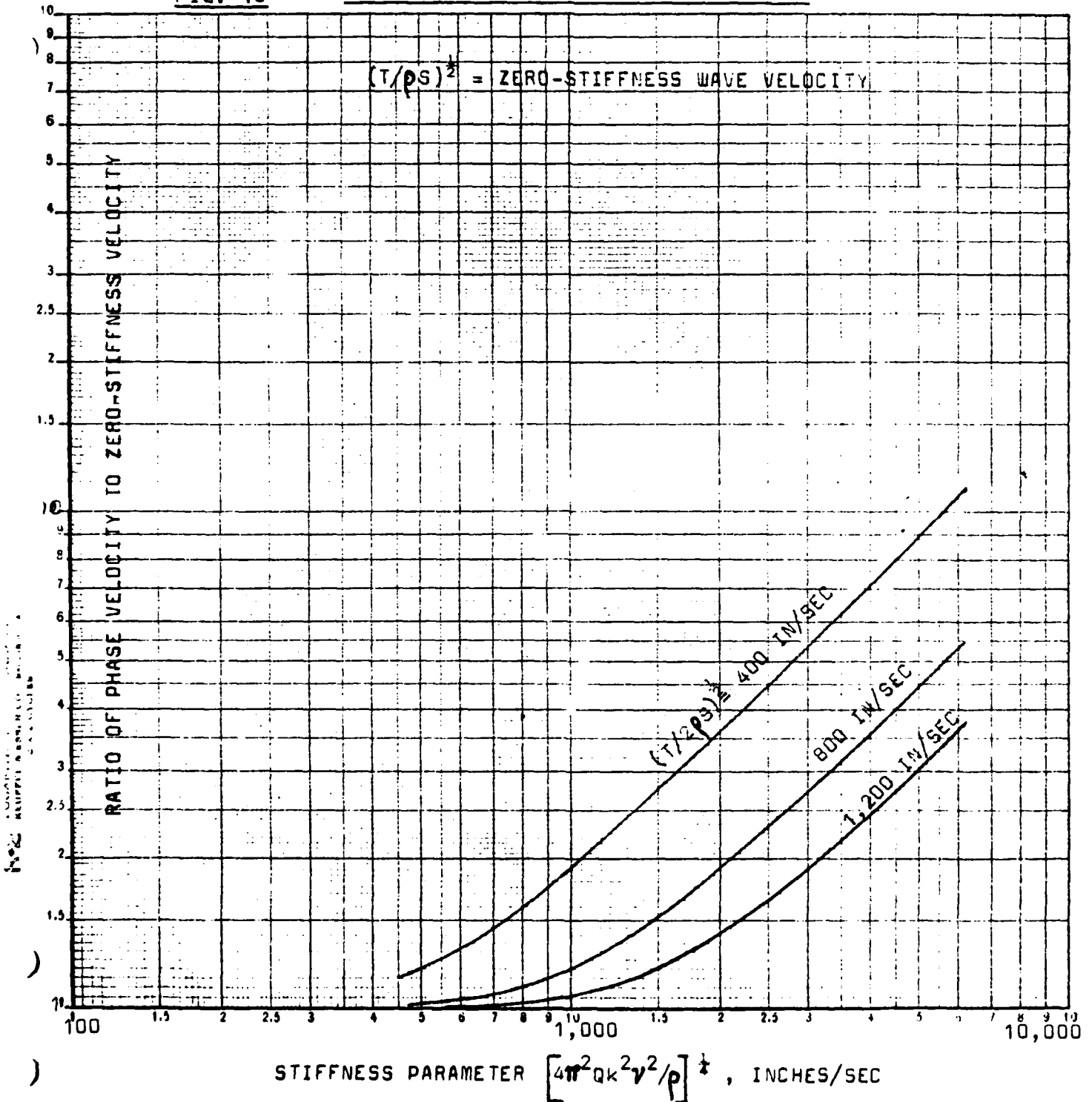| Ribbon Length, in.	22.5	15.0	10.0
Straight Bridge, ms	45.3	37.8	29.7
Standing Wave , ms	26.2	18.0	12.3

TABLE 11   UNWINDING PREDICTION COMPARISON

Table 11 shows that unwinding times predicted by the standing wave model are approximately half those predicted by the straight bridge model.

Effects of ribbon stiffness on standing wave velocity may be estimated from Fig.13, which has been calculated from equations given by Morse (Ref.4). In Morse's notation Q is modulus of elasticity, k is the radius of gyration of the ribbon's section (equal to $h/(12)^{\frac{1}{2}}$), γ is the forcing

FIG. 13   PHASE VELOCITY OF WAVES IN A RIBBON

$(T/\rho s)^{\frac{1}{2}}$ = ZERO-STIFFNESS WAVE VELOCITY

RATIO OF PHASE VELOCITY TO ZERO-STIFFNESS VELOCITY

$(T/2\rho s)^{\frac{1}{2}}$ 400 IN/SEC

800 IN/SEC

1,200 IN/SEC

STIFFNESS PARAMETER $\left[4\pi^2 Q k^2 \gamma^2/\rho\right]^{\frac{1}{2}}$, INCHES/SEC

- 46 -

frequency (equal to ω), and ρ is density. For aluminum, the stiffness parameter used as the abscissa of Fig.13 is as follows (ω= 3142 rad/sec as in the previous examples):

$$\text{Stiffness} = \left[4\pi^2(10^7)\frac{h^2}{12} \frac{(3142)^2}{.10}/386\right]^{\frac{1}{4}} = 33,500\ h^{\frac{1}{2}},\ \text{in/sec}$$

In Table 12, stiffness parameters are applied to the 15 inch ribbons analyzed above in three different thicknesses. In each case the standing wave velocity is taken to be twice that calculated with the straight bridge model, for order of magnitude estimates.

h, inches	.002	.004	.006
Stiffness Parameter, in/sec	1,500	2,100	2,600
Est. $(T/\rho S)^{\frac{1}{2}}$=L_o/t, in/sec	621	794	993
$(T/2\rho S)^{\frac{1}{2}}$	439	561	702
Approx. Velocity Ratio, from Fig.13	2.6	3.0	3.0

TABLE 12   EFFECTS OF STIFFNESS ON V_s

Table 12 indicates that stiffness can have a profound influence on unwinding speed, confirming the empirical observation that only dead-soft materials are suitable for ribbons. To isolate the effect of ribbon thickness on V_s is a difficult task, however, since Fig.13 shows that such effects will depend on the magnitude of the stiffness parameter. At low values of the stiffness parameter, variations in h will have little effect.

Both theoretical models discussed above will be compared with empirical data. Absolute predictive capabilities will be calculated, as well as the abilities of the models to predict trends in unwinding times as affected by material, geometry, and other parameters. To aid in this evaluation process, total unwinding times have been calculated and plotted in Fig.14. Average values of r and r_c during the unwinding process have been employed in calculating Fig.14, in order to avoid the step-by-step calculations such as those given in Tables 7-9. This averaging approach does not introduce excessive inaccuracy in Δt, and Fig.14 will be employed for comparing theoretical models with empirical results.

4.3 Correlations with Empirical Data

Fig.15 presents the empirical data obtained in this program (Section 2, Table 1) in the format suggested by the analytical models, i.e., $r_{co}\omega\Delta t/L_o$ vs. $hL_o/4\pi r_1 r_{co}$. To a first approximation, ribbon material does not seem to have much effect despite wide variations in density (from aluminum to lead) and other properties. Accordingly, a single curve is faired through the scattered data points. This curve is plotted in Fig.16 for comparison with the predictions of the two analytical models at the experimental $r_{co}/r_1 = 2.51$.

Fig.16 shows no distictly better predictive accuracy of one model over the other, with the empirical data falling between the two predictions at $r_{co}/r_1 = 2.51$.

In regard to the effects of r_{co}/r_1, which is predicted by·the straight bridge model to have major effects and by the standing wave model to have relatively minor effects (see Fig.14), it is unfortunate that this distinct difference

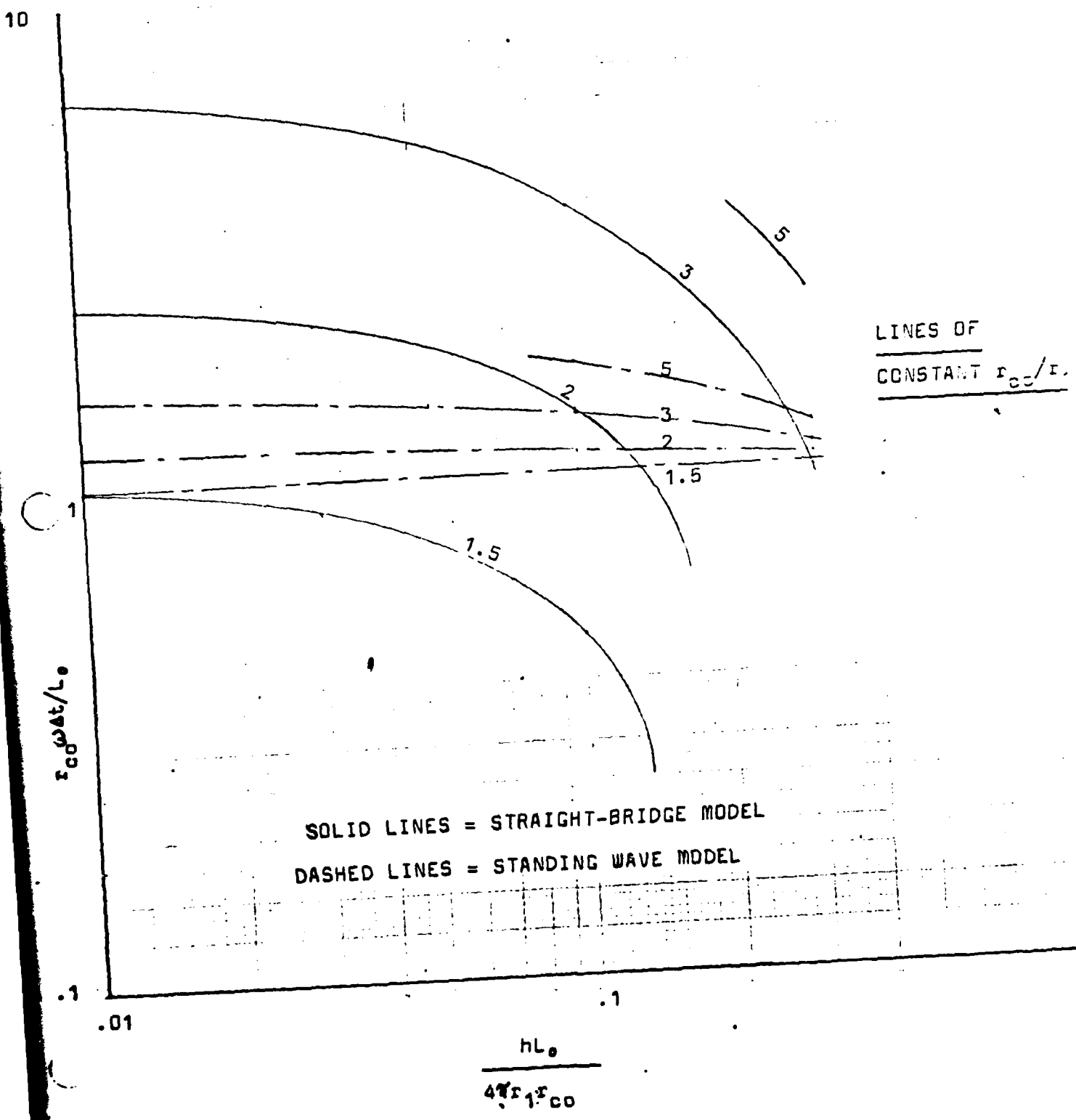FIG. 14   TOTAL UNWINDING TIMES

SOLID LINES = STRAIGHT-BRIDGE MODEL

DASHED LINES = STANDING WAVE MODEL

LINES OF

CONSTANT r_{co}/r.

- 49 -

FIG. 15   AIR SPINNER DATA WITH $r_{co}/r_1 = 2.51$

⊙ ALUMINUM
● LEAD
✕ BRASS
▯ COPPER
✛ BERYLLIUM-COPPER

$r_{co} \omega \Delta t / L_o$

$h L_o / 4 \pi r_1 r_{co}$
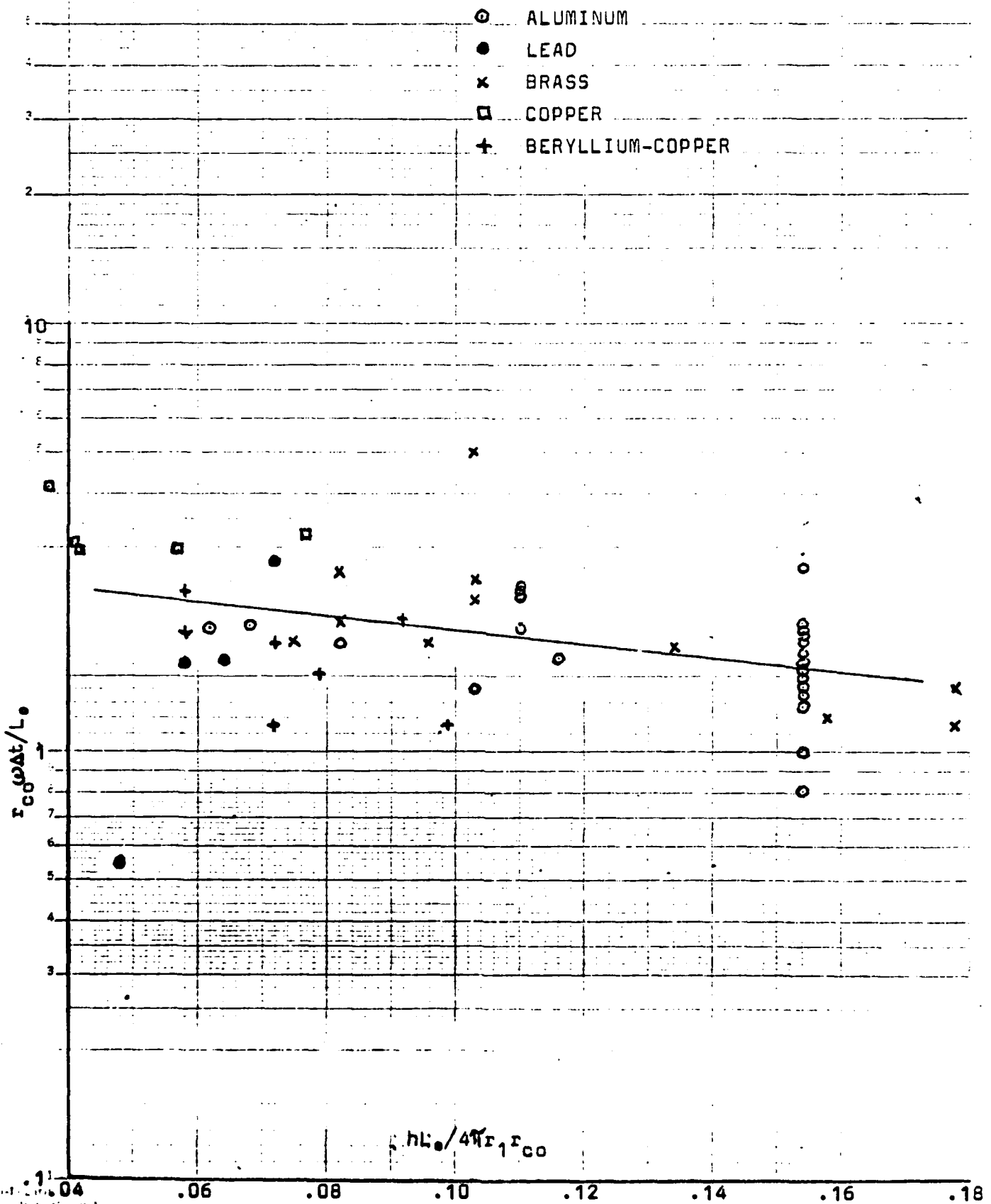
FIG. 16

FIG. 16 COMPARISON OF MODELS AND DATA AT $r_{co}/r_1 = 2.51$

STRAIGHT-BRIDGE MODEL

DATA

STANDING WAVE MODEL

$r_{co}\omega\Delta t/L_o$

$\eta L\dot{\omega}/4\pi r_1 r_{co}$

.04   .06   .08   .10   .12   .14   .16   .18
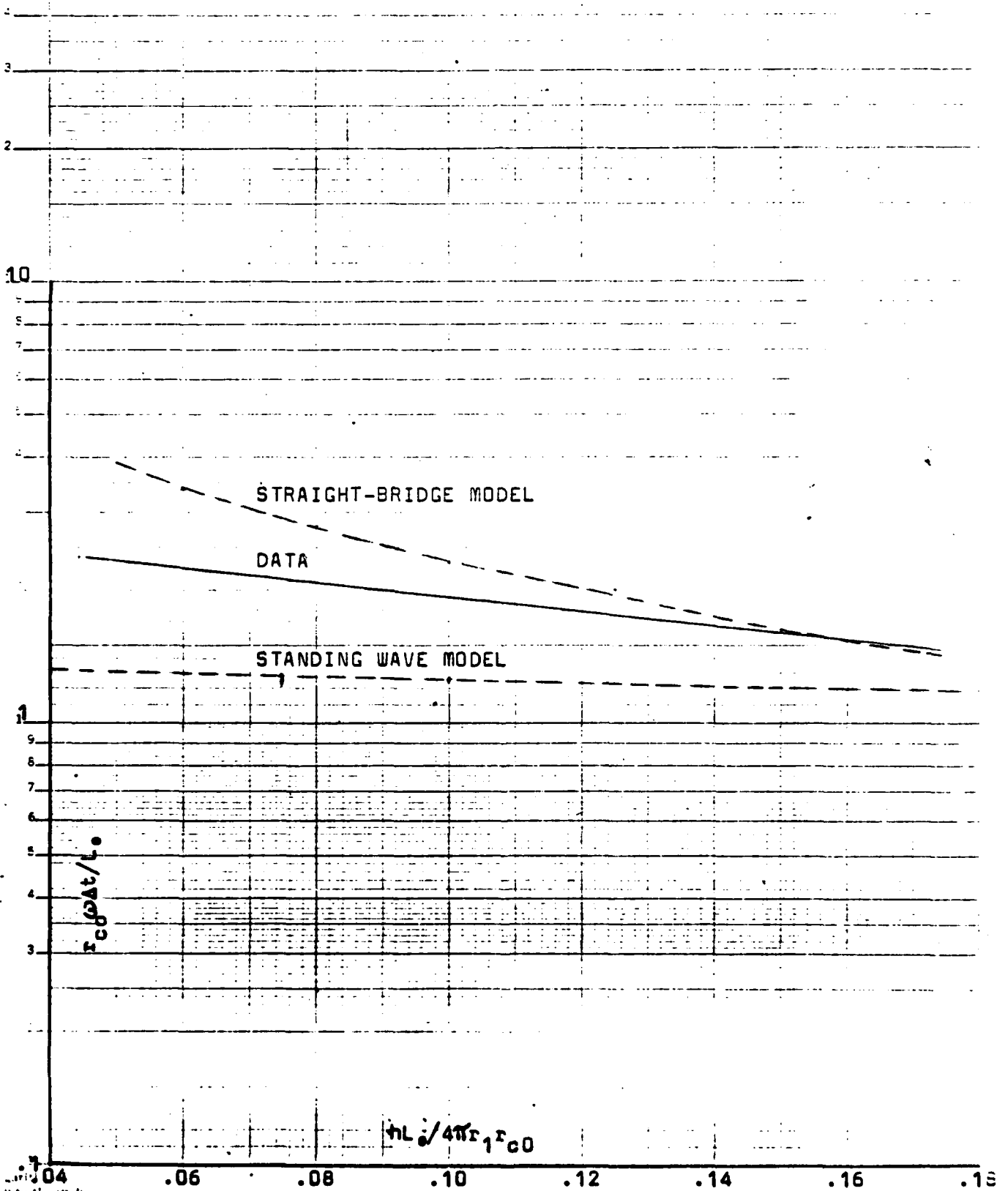
between the models cannot be evaluated on the basis of the r_{co}/r_1 = 2.51 air spinner data. The comparison of models can be made, however, on the basis of previously obtained data (Refs. 1,2) summarized in Table 2. These data are plotted in Fig.17 in groups of data, with each group having a constant r_{co}/r_1. Omitting for the moment the gun-fired unwinders and the with-liner ribbons (two thicknesses of .010 inch teflon liners between the hub and the innermost ribbon coil) which exhibit very high values of $r_{co}\omega\Delta t/L_o$, the remainder of the data tends to show negligible effects of r_{co}/r_1 in the 2.68 to 5.36 range. This lack of dependence on r_{co}/r_1 agrees with the standing wave model but conflicts with the predictions of the straight bridge model (see Fig.14).

Despite the reasonably good agreement between empirical data and the predictions of the standing wave model, this agreement does not establish the standing wave model as a physically complete description of ribbon dynamics. A basic dynamic analysis of ribbon motions during the unwinding process is required to establish the bridge shape, and how it may change as unwinding progresses.

4.4 Predictive Formula for Unwinding Time

Since Fig.17 shows that $r_{co}\omega\Delta t/L_o$ is practically independent of r_{co}/r_1, and the faired curve of Fig.16 shows a rather small effect of $hL_o/4\pi r_1 r_{co}$ (in the .04 to .18 range), it would appear that use of a mean value of $r_{co}\omega\Delta t/L_o$ may be adequate for purposes of designing ribbon unwinders. The air spinner data (Table 1) has a mean value of $r_{co}\omega\Delta t/L_o$= 1.95, which leads to the following equation for unwinding time:

EFFECTS OF r_{co}/r_1 ON UNWINDING TIME

FIG. 17
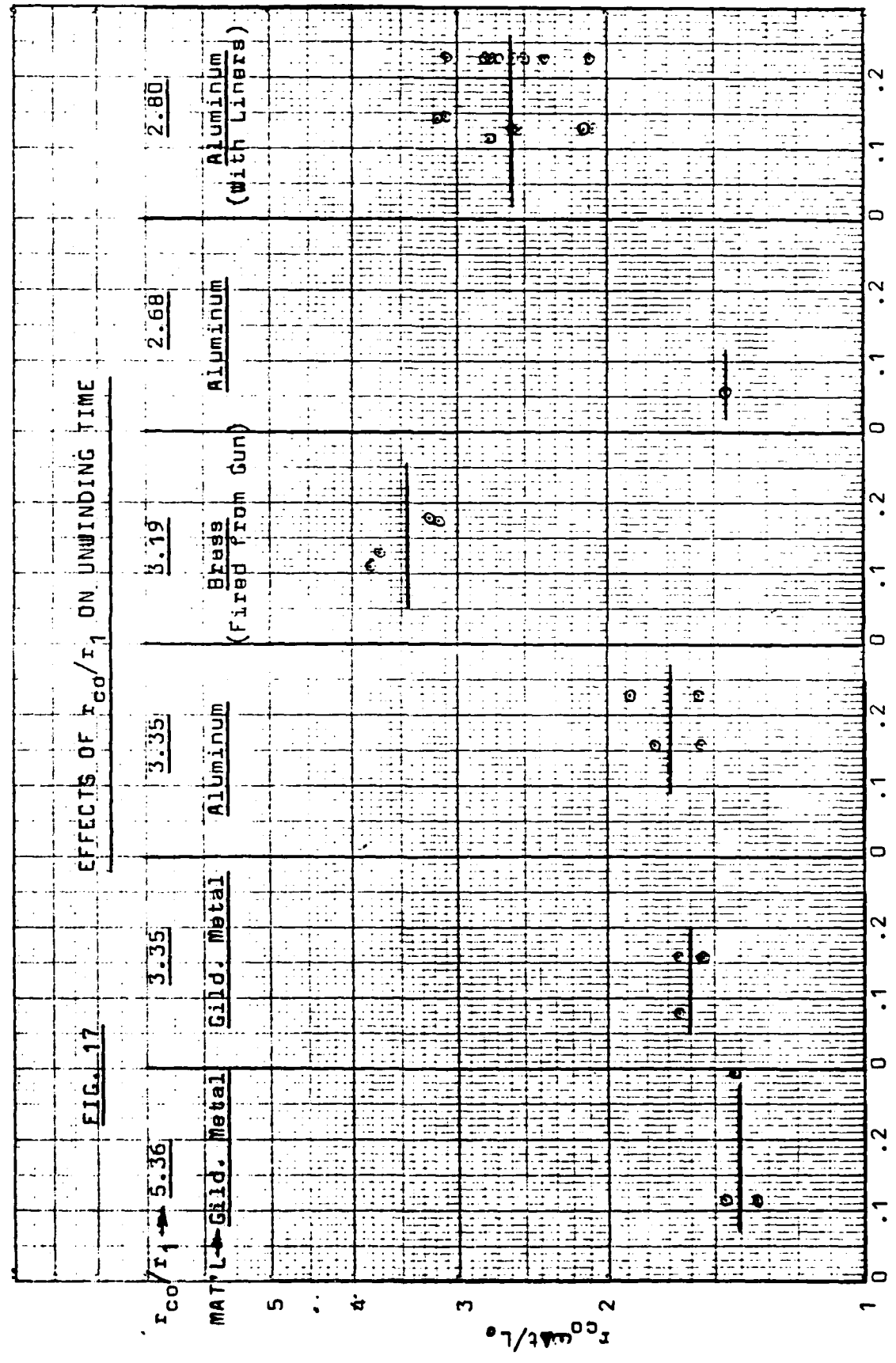
Unwinding Time $\quad \Delta t = 1.95 L_0 / \omega r_{co}$ $\qquad$ Eq. (28)

Applying Eq. 28 to all the empirical data gathered
in this air spinner test program, it is found that the
standard deviation is 0.76*. Since arming time requirements
generally permit greater variability than standard deviation
divided by mean = 0.76/1.95 = 0.39, Eq. 28 appears entirely
adequate for designing ribbon unwinders for arming delay
systems.

An interesting consequence of the form of Eq. 28 is
that arming distance is a constant, regardless of muzzle
velocity. For rifling with nd axial travel per revolution
of the projectile (where d is projectile diameter) muzzle
velocity = $\omega dn/2\pi$. Distance S_a where arming occurs is
muzzle velocity times Δt, or $\omega dn\Delta t/2\pi$. Since $\omega \Delta t$ =
$1.95 L_0/r_{co}$ from Eq. 28:

$$S_a/d = .31n(L_0/r_{co})$$ $\qquad$ Eq. (29)

Further, as an order-of-magnitude generalization,
d/r_{co} will be approximately equal to 4:

$$S_a \cong nL_0$$ $\qquad$ Eq. (30)

For n between about 20 and 40, the arming distance
of a ribbon unwinder will be of the order of 30 times the
ribbon length.

---

* The ALN analysis (Chap. 3) showed that the data could
not have resulted from random fluctuations. Therefore,
calculating a "standard deviation" based on a normal distribution
is not a rigorous procedure. However, applying this non-rigorous
approach to Eq. 2 results in "standard deviation"/mean = 0.42.

5. CONCLUSIONS & RECOMMENDATIONS

The primary objective in this program of developing methods of designing ribbon unwinders has been to derive usable equations for predicting unwinding time. This objective is fulfilled to a good enough approximation by Eq. 28, which gives reasonable accuracy with only the parameters of ribbon length and outer cavity radius and spin rate, and to better accuracy by Eq. 2 which uses additional ribbon parameters. There is no doubt that these preliminary design equations can be improved by more comprehensive programs of experimentation and analysis, but it is believed that the methods developed here are accurate enough for evaluating the relative advantages of using a ribbon unwinder as a delay element in a particular application. Further refinement of these equations is recommended, however, in view of the small data base used in their development.

It must be emphasized that unwinding time is not the sole criterion for selecting ribbon material and thickness. Aluminum 1100-0 is considered an excellent material because of its dead soft condition without requirement for annealing. Lead is also quite soft; however, the consensus is that it is too soft to handle as a practical fuze component. Likewise, foil below about .002 inches (.05 mm) in thickness may prove difficult to handle and may also be susceptible to edge damage during setback.

Ribbons with a high thickness-density product may be required in some applications to overcome the adhesive stresses between the coil layers. Table 1 contains the examples of .0012 inch (.030 mm) aluminum that did not unwind at spin rates of the order of 30,000 rpm, .0015 inch (.038 mm) copper that did not unwind at 20,000 rpm, and

.004 inch (.102 mm) aluminum that did not unwind at 15,000
rpm. Calculations of the centrifugal stresses at the
outermost layer of the ribbon coil ($r\omega^2\rho h$) were in the
0.5 to 1.0 psi range, and it is assumed that the adhesive
stresses between the outermost ribbon turn and its adjacent
turn were somewhat higher, thus preventing the ribbons from
unwinding. Comparable data available from previous programs
are 2.4 psi for a .006 inch (.152 mm) aluminum ribbon (Ref.1)
and 7.4 psi for a .004 inch (.102 mm) brass ribbon (Ref.2).
Inter-coil adhesive stresses are undoubtedly affected by
the surface condition of the ribbon, and it may well be that
the relatively low stresses obtained in this program were
due to the use of magnesium oxide on one side of each ribbon
to assist in annealing. In any event, it may be a practical
necessity to measure inter-coil adhesive stress for each
candidate ribbon material and then make sure that $r\omega^2\rho h$
exceeds the measured stress.

Ribbon unwinders appear to offer such good advantages
as delay elements that a considerable amount of effort to
develop unwinder technology is recommended. Some promising
areas of study that can be expected to broaden the data
base and to yield further insights into the behavior of
ribbon unwinders are as follows:

(1) Development of a computer model of ribbon
unwinder dynamics, including bending stiffness and adhesive
stresses and friction, from the time of release of the
ribbon's free end until the entire ribbon is transferred
to the outer cavity wall.

(2) Spinner experimentation with variations in the
parameters that were held constant in this program, particularly
hub and cavity radius.

(3) Setback experimentation that may reveal the
time delay required to spin up the coil, any effects of
setback on the edges of the ribbon, and any effects the
shock and vibration environment inside the spinning pro-
jectile may have on the ribbon unwinding process.

Perhaps the single most important reason for continuing
careful analytical and experimental programs such as the
above is that much-needed experience will be gained with
an arming delay system that shows such promise.

APPENDIX A

ADAPTIVE LEARNING NETWORK METHOD

Adaptive Learning Networks (ALNs) is an area of Artificial Intelligence that is concerned with producing phenomenological models of physical processes. The method for producing ALN models has been highly developed by ADI and has been successfully applied to such modeling problems as detection, classification, parameter estimation, prediction, process control, and others. For the ribbon unwinding data, the ALN can be used to model the unwinding time.

The classical approach to problems of detection, classification, estimation, etc. has been to determine explicitly all of the relevant characteristics (deterministic and/or statistical) of the observed process and to use those measurements and assumptions in the synthesis of a model. Often, the mathematical structure of the true process is assumed and the design process consists of calculating the coefficients of the model equations.

In many cases, the inputs or observables cannot be related to the output of the process in an analytical fashion. Further, the best or even an acceptable structure for the model cannot be determined a priori. These facts often result in linear models being used simply because the mathematics of such models are tractable.

However, it is often desirable to implement the model of a particular process as a general (usually nonlinear) function of certain input variables, the observables or features. Since the details of the relationships between the input variables and the output variable (the output process) are not known, the parameters and structure of the model are not known a priori. Rather, the model has to be "trained" from a data base of representative inputs and corresponding outputs.

To achieve trainability, the Adaptive Learning Network procedure uses, as a model of the observed process, a network of similar elementary building blocks. The training, or model synthesis, process determines the number of the elementary building blocks, the interconnections between them, and the parameters in each. In this way, the structure and coefficients of the model are derived from observations of the process. In order to implement such a scheme, the following questions need to be considered: First, what should the structure of the elements of the network be? Second, how should the element parameters be adjusted; and third, how should the elements be interconnected and what should be their complexity (i.e., number)?

These questions can be more clearly understood as follows: suppose that the process input consists of N observables, x_1, x_2, ..., x_N. Also, suppose that the output y is a scalar whose value may be considered as the estimate of some property of the input process. For the present application, that value is the ribbon unwinding time.   In general, y will be some nonlinear function of the x_i's, as follows:

$$Y = f(x_1, x_2, ..., x_N) \qquad\qquad (A.1)$$

Under fairly general conditions, a function of N variables may be expressed in an N-dimensional series as follows:

$$y = a_0 + \sum_{i=1}^{N} a_i x_i + \sum_{i=1}^{N} \sum_{j=1}^{N} a_{ij} x_i x_j + \sum_{i=1}^{N} \sum_{j=1}^{N} \sum_{k=1}^{N} a_{ijk} x_i x_j x_k + \cdots \qquad (A.2)$$

In the most general case, the coefficients, a_0, a_1, ..., are functions of time, but for many cases of interest, the underlying characteristics of the x's do not depend on time and, consequently, the coefficients are constants.

The above-stated questions can now be restated in terms of Equation (A.2) as follows: What elemental polynomial of the x_i's can be chosen such that, when its coefficients are adjusted and when several of them are interconnected, the resulting network is a good approximation to Equation (A.2) for the process of interest? Experience has shown that the element polynomials can be chosen to be either two-input or three-input devices. The three-input element implements a nonlinear function of inputs x_1, x_2, and x_3:

$$y = w_0 + w_1 x_1 + w_2 x_2 + w_3 x_3$$

$$+ w_4 x_1 x_2 + w_5 x_1 x_3 + w_6 x_2 x_3$$

$$+ w_7 x_1^2 + w_8 x_2^2 + w_9 x_3^2 \qquad (A.3)$$

$$+ w_{10} x_1 x_2 x_3 + w_{11} x_1^3 + w_{12} x_2^3 + w_{13} x_3^3$$

To reduce computational complexity, only one element of each layer of the network is allowed to use three inputs. Most elements contain only two inputs (x_1, x_2) such that:

$$y = w_0 + w_1 x_1 + w_2 x_2 + w_4 x_1 x_2$$

$$+ w_7 x_1^2 + w_8 x_2^2 + w_{11} x_1^3 + w_{12} x_2^3 \qquad (A.4)$$

A network of two layers of basic elements can contain products up to the ninth degree. Thus, fairly complex multinomials can be built up in a few network layers. To implement a fully general multinomial as in Equation (A.2), the number of elements in each layer would have to grow as one adds additional layers to the network. However, it has been found empirically that for most physical processes, acceptable networks can be obtained without such growth; in fact, the number of elements in successive layers decreases, and only a few layers are needed in the final network.

The coefficients in Equations (A.3) and (A.4), the w_i's are determined for each element individually by least squares fitting the desired or observed output y to the chosen inputs, x_i. The process of determining these coefficients and the number and interconnection of the individual elements is called the training of the ALN. These tasks are accomplished with a data base, for which the values of the dependent and independent variables are known. The steps involved in this process are:

    (1) optimization of the coefficients in each element of the first layer;

    (2) selection of those elements whose output is acceptable while rejecting poor performers;

(3) repetition of the first two steps for consecutive layers of the network;

(4) determination of the optimum number of network layers; and

(5) global optimization of all coefficients in all layers.

There are two ways in which step 4, the determination of the optimum number of network layers, can be performed. The first is an empirical technique which requires that the known data base be divided into three independent but statistically similar subsets called the fitting, selection, and evaluation subsets. The second technique makes use of an information theoretic criteria and requires only two subsets, a fitting subset and an evaluation subset. The division of the data base into subsets is accomplished with the Mucciardi-Gose clustering algorithm (Mucciardi and Gose, 1972). In both cases, the fitting subset is used to determine the coefficients of the elements. For the information theoretic criteria approach, the fitting subset is also used to reject those features that perform poorly. For the empirical approach, the selection subset is used to reject the poor performers and to prevent overfitting. Also, for that case, the fitting and selection subsets are used for the global optimization. The purpose of the evaluation subset is to estimate the overall performance. Since the evaluation subset is not used for network synthesis, the performance of this subset is an accurate estimate of the ability of the network to generalize to new, previously unseen data.

Consider, for the following, that each element has only two inputs and that the empirical technique for the determination of the correct number of layers in the network is being used. Then the fitting and selection subsets are used alternately in training each layer. First, the N-specific observables are arranged into N(N-1)/2 pairs, feeding a like number of trainable elements. Then the fitting subset of the known data base is applied to establish the coefficients, using a recursive search procedure to minimize the error rate between the independent variables and the output of the basic elements. The procedure is repeated for each of the N(N-2)/2 elements. Not all pairwise combinations are significant in extracting the desired information. The selection process, using the selection subset, eliminates those elements whose performance is not acceptable, as gauged by the error criterion. There are now, say, R elements that survive. The process is repeated for the second

- 61 -

layer. The observables now consist of the outputs of the surviving elements as well as the original independent variables. Coefficients of each element in the second layer are determined as in the first layer. Then the selection subset is fed a second time into the first layer and the unacceptable pairs eliminated from the second layer.

This process can be repeated with succeeding layers. In addition to eliminating the poorly performing features, the selection set is also used for determination of the optimum number of layers. The selection set should be used for this purpose because the error rate on the fitting subset could be continuously decreased by incorporating additional layers. Overfitting of the fitting subset occurs when the error rate on the selection subset starts increasing. Avoidance of overfitting is a key aspect in the training of learning networks (Ivakhnenko, 1971; Mucciardi, 1972). The network must be thought to generalize properly on its experience in fitting the points in the fitting subset, so that error rates in later uses for statistically similar data will also be low. The network may produce deceptively small errors in approximating the fitting subset and then do poorly on subsequent new data when overfitting is not avoided.

The growth of the model, i.e., the increase in the number of coefficients, can also be controlled by the use of an information criterion such as AIC, also called Akaike's information criterion (Akaike, 1973 and 1980; Kondo and Tamura, 1980; Tamura and Kondo, 1980). AIC measures the poorness of the model and, consequently, needs to be minimized:

$$AIC = 2\ell n(\text{maximum likelihood}) + 2(\text{number of coefficients}) = \text{minimum}. \quad (A.5)$$

In this case, the resulting model is called the minimum AIC model (MAIC). AIC is an estimate of twice the negentropy: thus a realization of the MAIC model is equivalent to the finding of that model from all possible models which possess the maximum entropy. AIC has also been used in autoregressive analysis techniques, such as spectral estimation; the optimal length for the prediction filter can be determined by applying AIC (Ulrych and Bishop, 1975; Landers and Lacoss, 1977).

When the appropriate number of layers has been found, the last layer will, in general, comprise a plurality of elements, each capable of producing an estimate of the dependent variable. These estimates may be numerically weighted and summed, or the single element that produces the lowest error rate vis-a-vis the selection subset may be retained, while all other parts of the network not needed to feed the surviving output element or elements are discarded.

A final step in the training process is the global optimization, also called vernier adjustment, of the coefficients. This may be desirable because the coefficients of each element have been adjusted in the absence of interactions with other elements following them in the network; optimum coefficient values may be slightly different from those determined earlier when these interactions are present. Fitting and selection subsets are also used for this final adjustment process. The vernier adjustment uses a random technique to obtain the optimum values of the coefficients, as well as for subsequent network adaptation. After final adjustment of the coefficients, the evaluation subset is used to estimate performance of the entire network.

In summary, the ALN technique is an empirically-based technique to obtain the structure of a process and does not require a priori principles and/or assumptions to be made about the process itself. Since both the structure of the model and the values for the model coefficients are obtained from the experimental data base, the ALN method is applicable to multi-sensor integration, detection classification, prediction, and the control of a wide range of complex physical, biological, and engineering processes. Application of ALN modeling has been successful even when theoretical or conventional modeling techniques produced insufficient results.

REFERENCES

1. Raff, B. and R.J. Caruso "Design and Development of
   Fuze, PIBD, XM579" Bulova Final Report, 19 Dec. 1969.

2. Tevelow, F.L. "Terminal Report - T362 Octopus Fuze"
   Diamond Ordnance Fuze Laboratory Report TR-673,
   10 August 1959.

3. Alfriend, T.B. "Study of Wrapped Springs for Application
   to a Delayed Arming Mechanism" Aircraft Armaments Inc.
   Report No. ER-1404, June 1958.

4. Morse, P.M. "Vibration and Sound", McGraw-Hill, Second
   Ed., 1948.

5. Hogg, R.V. and A.T. Craig "Introduction to Mathematical
   Statistics", Second Ed.,p. 291, McMillan, New York, 1965.